SAND2016-8497R

March 2016

PNNL- 25385 / SAND2016-XXXX

Model Test Bed for Evaluating Wave Models and Best Practices for Resource Assessment and Characterization

V.S. Neary
Z. Yang
T. Wang
B. Gunawan
A.R. Dallman

Prepared by

Pacific Northwest National Laboratory
Richland, Washington

and

Sandia National Laboratories
Albuquerque, New Mexico

Pacific Northwest National Laboratory is the U.S. Department of Energy's premier chemistry, environmental sciences, and data analytics national laboratory—managed and operated by Battelle since 1965, under Contract DE-AC05-76RL01830, for the DOE Office of Science.

Sandia National Laboratories is a multi-program laboratory managed and operated by Sandia Corporation, a wholly owned subsidiary of Lockheed Martin Corporation, for the U.S. Department of Energy's National Nuclear Security Administration under contract DE-AC04-94AL8500.

DISCLAIMER

PACIFIC NORTHWEST NATIONAL LABORATORY
operated by
BATTELLE
for the
UNITED STATES DEPARTMENT OF ENERGY
under Contract DE-AC05-76RL01830

Printed in the United States of America

Available to DOE and DOE contractors from the
Office of Scientific and Technical Information,
P.O. Box 62, Oak Ridge, TN 37831-0062;
ph: (865) 576-8401
fax: (865) 576-5728
email: reports@adonis.osti.gov

Available to the public from the National Technical Information Service
5301 Shawnee Rd., Alexandria, VA 22312
ph: (800) 553-NTIS (6847)
email: orders@ntis.gov <http://www.ntis.gov/about/form.aspx>
Online ordering: http://www.ntis.gov

This document was printed on recycled paper.
(8/2010)

PNNL- 25385 / SAND2016-XXXX

Model Test Bed for Evaluating Wave Models and Best Practices for Resource Assessment and Characterization

Vincent S. Neary[1]
Zhaoqing Yang[2]
Taiping Wang[2]
Budi Gunawan[1]
Ann R. Dallman[1]

March 2016

Prepared by

[1]**Sandia National Laboratories**
Water Power Technologies

and

[2]**Pacific Northwest National Laboratory**
Coastal Sciences Division

for the U.S. Department of Energy

Summary

A wave model test bed is established to benchmark, test and evaluate spectral wave models and modeling methodologies (i.e., best practices) for predicting the wave energy resource parameters recommended by the International Electrotechnical Commission, IEC TS 62600-101Ed. 1.0 ©2015. Among other benefits, the model test bed can be used to investigate the suitability of different models, specifically what source terms should be included in spectral wave models under different wave climate conditions and for different classes of resource assessment. The overarching goal is to use these investigations to provide industry guidance for model selection and modeling best practices depending on the wave site conditions and desired class of resource assessment. Modeling best practices are reviewed, and limitations and knowledge gaps in predicting wave energy resource parameters are identified.

Third generation (3G) spectral wave models are evaluated, including WaveWatch III with the ST2 physics package (WWIII ST2), WWIII with the ST4 physics package (WWIII ST4), SWAN with open-wave boundary inputs from WWIII (ST2), and SWAN with open-wave boundary inputs from WWIII (ST4). Modeling methodologies and best practices are reviewed, and limitations and knowledge gaps in predicting wave energy resource parameters are identified. A nested structured grid approach is employed to provide open-wave boundary conditions to a 60 km x 60 km local model domain. Model performance, aka *model skill*, is defined by evaluating half-a-dozen standard performance metrics based on a comparison of the predictions of six IEC wave resource parameters derived by model hindcasts to those derived from buoy measurements. Potential improvements in model performance, e.g., those due to increased spectral resolution, are quantified by comparing these same metrics with baseline model test cases. The baseline model test cases are designed to meet or exceed IEC TS 62600-101Ed. 1.0 requirements for *feasibility class* resource assessments. The test bed grid size is 12" x 10" (~300 m), simulated two-dimensional wave spectra are predicted hourly, and discretized with 29 frequency bins and 24 direction bins, using a logarithmic increment factor of 1.1, and a minimum frequency of 0.035 Hz, which gives the maximum frequency of 0.505 Hz. NOAA/NCEP CFSR data, at 0.5-degree (~50 km) spatial resolution and hourly intervals, is used for wind forcing. All models employ source terms for *design class* resource assessments, including terms for linear and exponential wind growth, and dissipation terms that simulate whitecapping, quadruplet wave interaction, wave breaking and bottom friction. Default parameter settings for these source term models are used; i.e., no coefficients in any source terms are calibrated to measurements.

For the baseline model test case, a comparison of the six IEC parameters time series indicates good agreement between WWIII simulations and NDBC buoy measurements at a depth of 128 m. Predicted time series for these six parameters from the SWAN model, both in nonstationary and stationary modes, are comparable to those from the present study's WWIII (ST2) model; and likewise provide confidence in the SWAN model settings. Only small differences between WWIII and SWAN predictions are observed. Increasing the spectral resolution, specifically almost doubling the number of frequency bins, and increasing the direction bins by 50 percent, is found to provide no improvement in WWIII or SWAN model skills, but this insensitivity was likely due to the large depth (128 m) at the point of comparison and the absence of any bathymetric or geometric features in the vicinity. Better representations of growth and dissipation, specifically when modeling swell dissipation effects with the WWIII ST4 physics package, generally improve model performance. Notably, model skill for predicting omnidirectional wave power density and significant wave height, for average and large waves, is significantly improved. In contrast, model skill for predicting energy period is slightly reduced when modeling swell dissipation effects.

The present study is limited to a structured grid model skill evaluation at a deep offshore wave site and default model settings. Future studies should investigate model performance in shallow nearshore environments, and the benefits of model calibration, particularly for improving predictions of energy period with the WWIII ST4 physics package, and for improving predictions of large waves. In addition, it is important to investigate the benefits of more accurate wind forcing inputs, particularly for large wave prediction. The model skill evaluation should be extended to include the comparison of predicted and measured wave spectra. The model test bed can also facilitate investigation of the benefits of unstructured-grids (over a large model domain of interests).

,

Acknowledgments

A steering committee, chaired by Dr. Tuba Özkan-Haller, Professor at Oregon State University and wave modeling expert, was organized to provide external oversight, input, and review for this model study, including recommendations on the selection of the common wave site to serve as the model test bed, and review of the model study plan and objectives. Steering committee members included two experts in wave modeling, one wave energy converter (WEC) industry representative, and one representative from the National Renewable Energy Laboratory (NREL). Dr. Bryson Robertson, program manager at the West Coast Wave initiative, Institute of Energy Systems, at the University of Victoria, is an international expert on wave modeling who was invited to participate because of his expertise in wave resource assessment and current work assessing the wave energy resource off the west coast of Canada. Dr. Arun Chawla, the other international expert on wave modeling, was invited to participate because he leads the WAVEWATCH III® (WWIII) model suite and applications development group at the National Oceanic and Atmospheric Administration's (NOAA) National Center for Environmental Prediction. Dr. Tim Mundon, a senior research and development engineer at Oscilla Power™, Inc., was invited because of his expertise in wave dynamics and WEC technologies. Dr. Levy Kilcher, an ocean engineer with the NREL, was invited because he is the principal investigator on a project sponsored by the DOE Wind and Water Power Technologies Office that is identifying primary sites for wave energy projects development based on resource availability and other economic criteria. Steering committee members participated in three scheduled calls with Sandia National Laboratories and Pacific Northwest National Laboratory, reviewed two drafts of the model study plan, and provided valuable input and recommendations that were adopted in this final draft of the model study plan.

Acronyms and Abbreviations

3G	third generation
AWAC	acoustic wave and current (profiler)
CFL	Courant–Friedrichs–Lewis
CFSR	Climate Forecast System Reanalysis
CHL	Coastal Hydraulics Laboratory
C-MAN	Coastal-Marine Automated Network
COAMPS	Coupled Ocean/ Atmosphere Mesoscale Prediction System
COC	Central Oregon Coast
CPU	central processing unit
DIA	discrete interaction approximation
EMC	Environmental Modeling Center
FVCOM	finite volume coastal ocean model
GB	gigabyte
GHz	gigahertz
Hz	hertz
IAHR	International Association of Hydraulic Research
IEC	International Electrotechnical Commission
JONSWAP	JOint North Sea WAve Project
km	kilometer(s)
km^2	square kilometer(s)
kW/m	kilowatt(s) per meter
m	meter(s)
MB	megabyte
MMAB	Marine Modeling and Analysis Branch
MIKE 21	2D hydrodynamic model named after Dr. Mike Abbott
MIKE 21 SW	MIKE 21's spectral wave module
msl	mean sea level
NCEP	National Centers for Environmental Prediction
NDBC	National Data Buoy Center
NETS	North Energy Test Site
Nm	nautical mile(s)
NNMREC	Northwest National Marine Renewable Energy Center
NOAA	National Oceanic and Atmospheric Administration
OS	operating system
PDF	probability density function
PMEC	Pacific Marine Energy Center

PNW	Pacific Northwest
POR	period of record
R&D	Research and Development
RMSD	root-mean-square-deviation
RMSE	root-mean-square-error
s	second(s)
SETS	South Energy Test Site
SI	scatter index
STWAVE	STeady State spectral WAVE
SWAN	Simulating WAves Nearshore
SWAN-NS	Nonstationary SWANmodel simulation
SWAN-S	Stationary SWAN model simulation
TB	terrabyte
TS	Technical Specification
WAM	WAve prediction Model
WEC	wave energy converter
WWIII	WAVEWATCH III
yr	year(s)

Contents

Figures

Tables

1.0 Introduction

1.1 Motivation

The recently published International Electrotechnical Commission Technical Specification on wave energy resource assessment and characterization (IEC TS 62600-101Ed. 1.0 2015) provides a standardized methodology to ensure wave resource assessment and characterization is performed consistently and accurately. This methodology relies primarily on spectral wave model hindcasts for deriving recommended wave energy resource parameters. It also includes best modeling practices depending on the desired class of resource assessment, e.g., model selection, minimum period of simulation, model boundary conditions, model resolution, model forcing resolution (e.g., wind forcing), and model validation. The goal of the present study is to establish a wave model test bed to benchmark, test and evaluate modeling methodologies, and model skill for predicting the IEC TS's recommended wave energy resource parameters. It reviews current wave modeling best practices, wave model codes, and limitations and knowledge gaps in predicting normal and extreme sea states, and recommends future research to improve wave modeling.

1.2 Wave Resource Assessment and Characterization

Wave energy resource is defined in IEC TS 62600-101Ed. 1.0 (2015) as "the amount of energy that is available for extraction from surface gravity waves." This technical specification defines three classes of resource assessment. Class 1, or *reconnaissance*, is the lowest level and produces estimates with high uncertainty. This level would be appropriate for large areas as the first assessment in a region. Class 2, or *feasibility*, produces estimates with greater certainty, and is appropriate for refining a reconnaissance assessment before a Class 3 assessment is done. Class 3, or *design*, produces an assessment with the least uncertainty and would be the final and most detailed assessment for small areas. For a detailed resource assessment at a particular site of interest, the IEC recommends that the energy assessment be based on the analysis of directional wave spectra observations from long-term buoys or be produced from a simulated hindcast. Measurements (e.g., those from buoys) can also be useful for specification of boundary conditions and model validations. The IEC TS 62600-101Ed. 1.0, and recent studies analyzing the wave resource off the U.S. Pacific Northwest coast (Lenee-Bluhm et al. 2011; García-Medina et al. 2014; Dallman and Neary 2014), recommend six parameters for characterizing the wave energy resource. These six parameters are omnidirectional wave power, significant wave height, energy period, spectral width, direction of maximum directionally resolved wave power, and the directionality coefficient.

As point measurements, buoy observations near the study site may not accurately reflect the wave climate at the site because of spatial and temporal constraints. They may not be in close enough proximity to the study site to be representative of the wave climate; or they may have an insufficient period of record (POR) to accurately characterize the wave climate statistics. The POR can be especially important for characterizing extreme sea states, as well as normal sea states when inter-period climate oscillations occur on the order of a few years or decades (e.g., Wang and Swail 2001; Vimont 2004). A minimum POR of 10 years is often recommended for characterizing normal sea states, and 20 years for extreme sea states (e.g., IEC TS 62600-101Ed. 1.0). However, it is rare to find buoy observations that are both representative of the wave climate at the study site, and with PORs greater than 10 years. Model hindcasts of the wave climate, therefore, offer an attractive alternative for characterizing wave energy resources.

Wave models have their own limitations. Even if a wave model captures all of the key physics (e.g., wave generation, growth, nonlinear interactions, dissipation, effects of currents), accurate modeling is still

dependent on the wave model selection (e.g., source terms selected in the phase-averaged wave models), specification of model inputs (e.g., wind data sources), proper model calibration and validation (e.g., challenges resulting from many calibration parameters, use of different metrics for evaluating model performance), the dependency of spatial and temporal model resolutions, and the frequency and direction resolutions of wave spectra. These same models generally over-predict significant wave heights and omnidirectional wave power during normal seas, which has been attributed to failure to accurately model swell dissipation effects (e.g., Ardhuin et al. 200), andan over-bias in wind forcing used to drive the wave models (e.g., Dallman et al. 2014).

Cavaleri (2009) summarizes the limitations of wave models to predict large waves, including those related to wave physics (e.g., more frequent underestimates of higher surface wind speeds, low-pass filtering of high wind speeds (smoothing) due to insufficient spatial resolution, failure to capture gusts, failure to capture wave shoaling effects of currents, and the breakdown of wave generation, whitecapping (breaking), and discrete interaction approximation (DIA) models at high wind speeds, those related to numerics, i.e., numerical diffusion caused by low-order numerical schemes and spatial, temporal and spectral (frequency and direction) resolution, and those related to modeling (e.g., model tuning or calibration).

When selecting models for wave resource characterization it is important to understand the key processes affecting wave dynamics near the shore where WEC projects are expected to be deployed. Wave dynamics in the nearshore zone include more complex phenomena than offshore regions, and the number of phenomena to be modeled generally increases across the surf zone towards the shoreline. As waves travel from deep waters into shallower regions, they become more nonlinear, transferring energy from the peak of the spectrum to higher and lower frequencies. Eventually, the proximity of the sea bottom will induce the breaking of the waves, producing a severe increase in the marine turbulence levels, and generating different types of currents, which may extend beyond the surf zone. Although the majority of WEC technologies are designed for nearshore deployments at depths between 50 and 200 meters, a number of WEC developers are also looking at shallower depths due to the lower costs of transmission cables. Therefore, it is prudent to evaluate the accuracy of wave model predictions at shallow depths (<30 m) as well; where more complex wave dynamics are occurring, and where bed-mounted WEC technologies (Drew et al. 2009) could potentially be deployed.

1.3 Review of Wave Models

A wide range of numerical models exist for simulating surface wave processes based on different physical assumptions and numerical frameworks. Wave models can be divided into two major categories: 1) deterministic (phase-resolving) models and 2) stochastic spectral (phase-averaged) models. Phase-resolving models are based on fundamental wave equations with rigorous approximations. The evolution of the sea surface is computed on a grid with a resolution finer than the wavelength. As such, these models are impractical for performing hindcast simulations for large model domains and long durations (~5 to 10 years) because of the high computational requirements. Phase-averaged models provide a statistical description of the wave conditions in space and time based on the wave energy balance equation, and compute the distribution of wave energy in frequency, direction, and its evolution in time at every grid point. These models are, therefore, the only practical models that can be employed for wave resource characterization.

Third-generation (3G) spectral models resolve the nonlinear interactions in the spectral wave energy equation (Tolman et al. 2014), and allow the simulation of sea states ranging from normal conditions to extreme storm conditions (e.g., hurricanes). Popular 3G phase-averaged wave models include SWAN, WAVEWATCH III® (WWIII), WAM, MIKE21 SW, TOMAWAC, and STWAVE. These 3G models

can be classified into structured-grid and unstructured-grid models. SWAN and WWIII are well documented, and are the most widely used models among all the 3G spectral wave models. Both have been applied for wave energy resource characterization (e.g., Dallman and Neary 2014; Dallman et al. 2014). The fundamental difference between WWIII and SWAN is the numerical scheme solving the spectral wave action balance equation. WWIII uses explicit schemes to advance the solution in time and space, while SWAN uses implicit schemes. However, an implicit scheme for WWIII is in development. In both models, users can select first- to higher-order accurate numerical schemes.

WWIII is maintained at the Marine Modeling and Analysis Branch (MMAB) of the Environmental Modeling Center (EMC) of the National Centers for Environmental Prediction (NCEP) (Tolman 2010; Tolman et al. 2014) as part of the National Oceanic and Atmospheric Administration's (NOAA's) marine operational forecast system. It was selected over WAM for use in Pacific hindcast simulations based on performance scores for predicting significant wave height, period, and direction, although overall performance results were relatively similar (Hanson et al. 2006). WWIII solves the phase spectral action density balance equation for wavenumber-direction spectra under various conditions. The current version 4.18 of WWIII (Tolman et al. 2014), which is available to the public, consists of a collection of physical packages, including curvilinear grids (Rogers and Campbell 2009), structured and unstructured-grids (Ardhuin and Roland 2013), various wind-wave interaction and dissipation packages such as ST2, ST4, and ST6 (Ardhuin et al. 2010; Tolman, 2014), and the effects of sea ice. Explicit numerical schemes (from first- to third-order) are used to solve the governing equation in WWIII for the traditional regular grids. Therefore, the model run time step is constrained by the Courant–Friedrichs–Lewis (CFL) stability criteria (CFL$\leq$1).

SWAN is a phase-averaged (spectral) model that solves the action balance equation using implicit numerical schemes (first- to second-order) to predict the wave statistics at each grid cell point within the model domain (The SWAN Team 2015). These implicit schemes allow larger time steps than models using explicit schemes, which allow computationally efficient simulations with grid cell sizes less than 1 km. SWAN models nearshore wave effects that include nonlinear wave interactions, refraction and shoaling due to bathymetry or ambient currents, and white capping and depth-induced breaking. As a result, SWAN is the most commonly used 3G spectral wave model for resource characterization (Dallman and Neary 2014; Dallman et al. 2014). In addition, SWAN can solve the steady form of the action balance equation by running in the stationary mode, which greatly reduces computational requirements and run times. This option is most appropriate when the model domain is sufficiently small (~100 km).

WAM is the first 3G spectral wave model developed by the WAMDI Group (WAMDI Group 1988); it simulates spectra of random wind-generated waves by solving the action density equation, including nonlinear wave-wave interactions similar to SWAN and WWIII. It is one of the most well-tested wave models and is widely used internationally, especially in European wave modeling communities. Currently, only a structured-grid version of WAM exists.

STWAVE (STeady State spectral WAVE), developed by the Coastal Hydraulics Laboratory (CHL) of the U.S. Army Corps of Engineers (USACE), is described as a half-plane model for nearshore wind-wave growth and propagation that simulates depth-induced wave refraction and shoaling, current-induced refraction and shoaling, depth- and steepness-induced wave breaking, approximated diffraction, parametric wave growth because of wind input, and wave-wave interaction and white capping that redistribute and dissipate energy in a growing wave field (USACE-CHL 2014, http://chl.erdc.usace.army.mil/chl.aspx?p=s&a=software;9). As a half-plane model, and in contrast to the models discussed above (e.g., SWAN), STWAVE currently does not have the capability to simulate propagation and generation from all directions.

FVCOM-SWAVE is a wave module embedded in the unstructured-grid, finite volume coastal ocean model (FVCOM; Chen et al. 2003). FVCOM-SWAVE retains all of the physics and options available for source terms in the SWAN model (Qi et al. 2009). The main difference between SWAN and FVCOM-SWAVE is the numerical scheme in solving the wave governing equation because FVCOM is built in unstructured-grid finite-volume framework. Because FVCOM-SWAVE is directly integrated with the FVCOM modeling system, it is more convenient in terms of simulating wave-current interaction and environmental impacts (Sun et al. 2013).

TOMAWAC is the commercial wave sub-module of the integrated TELEMAC modeling system (http://www.opentelemac.org/), which consists of sub-modules for hydrodynamics, sediment transport, and wave propagation. TELEMAC is designed to solve various free surface processes in oceans and coastal seas using finite element numerical methods in an unstructured-grid framework. Similar to SWAN and WWIII, TOMAWAC models the sea states by solving the balance equation of the action density directional spectrum (Gagnaire-Renou et al. 2010). TOMAWAC user groups are primarily based in European countries because the TELEMAC system was originally developed by the Laboratoire National d'Hydraulique et Environnement in France.

MIKE 21 SW is the commercial 3G spectral wave sub-module of the MIKE 21 modeling system that solves the action balance equations on an unstructured grid using a finite-volume method (Sørensen et al. 2004). Similar to SWAN, it simulates the effects of various physical effects on wave generation, propagation, and dissipation, including wind, nonlinear wave-wave interaction, and dissipation due to white capping, bottom friction, and wave breaking, and refraction and shoaling due to depth variations. It also can simulate wave-current interaction and the effect of time-varying water depth.

Although unstructured-grid models provide advantages in computational efficiency and flexibility for simulating wave climates near complex geometries, they are still relatively new compared to structured-grid models and are not well vetted. Publications on the development and applications of unstructured-grid 3G wave models (such as SWAN and WWIII) are limited (Zijlema, M. 2010; Robertson et al 2014; Qi et al. 2009; Ardhuin and Roland 2013).

1.4 Model Selection

Based on the review of wave models provided in the previous section, the present study was limited to comparing structured-grid versions of the two most widely used 3G phase-averaged models—WWIII (v4.18) and SWAN (v41.01). WWIII (ver. 4.18) is maintained by NOAA for real-time operation and long-term hindcasts at global and regional scales around the world. The theory and methods implemented in WWIII are fully documented (Tolman 2010; Tolman et al. 2014), and numerous peer-reviewed journal articles about WWIII modeling studies have been published, including modeling studies in the present study's model domain (e.g., García-Medina et al. 2014).

SWAN (ver. 41.01A) was chosen because it is the only documented and supported 3G model specifically developed to model nearshore effects. Whereas WWIII was originally designed and is generally used for wave modeling on ocean scales (spatial scales >500 km, model domains $>10^5$ km^2), SWAN is designed to run on coastal scales (shelf seas with model domains $<10^5$ km^2). Other 3G models reviewed, e.g., WAM, are generally not as well documented or supported as WWIII or SWAN. TOMAWAC and MIKE-21 SW are less popular models than WAM, WWIII and SWAN, and are not as fully vetted in the peer-reviewed literature.

1.5 Study Goals and Objectives

The goal of the present study is to establish a wave model test bed to benchmark, test and evaluate modeling methodologies, and model skill for predicting the IEC TS's recommended wave energy resource parameters. It reviews current wave modeling best practices, wave model codes, model source terms, and limitations and knowledge gaps in predicting sea states, and recommends future research to improve wave modeling.

As a model test bed the wave site was selected to be representative of a commercial wave energy resource site, and for which sufficient met-ocean data are available to allow a consistent assessment of different models, modeling methodologies and model inputs.

The accurate prediction of wave power density using 3G spectral models, arguably the most important metric of a site's wave energy resource, has been particularly challenging. Therefore, a comparison of predictions for these parameters using WWIII and SWAN (both nonstationary and stationary modes) on an identical structured model grid, along with the other IEC TS 62600-101ED 1.0 recommended parameters, provides an opportunity to investigate the causes of these current limitations and ways to improve model performance. For the present study, neither model is calibrated using a split-sample method. Only recommended default settings are used for all source term models.

For this initial phase, the present study conducted the following model investigations:

- Spectral resolution (frequency and direction): A high spectral resolution, both in frequency and direction, is important to accurately model the advection of energy from swell over long distances. A complex bathymetry and geometry in shallow-water regions, in particular, can alter the frequency-directional characteristic of incoming waves. Potential improvements in model predictions by increasing the number of frequency and direction bins are evaluated by comparing results to those predicted for a baseline model case.
- Swell dissipation (wave turbulence interactions): The limitation of most 3G wave models in accounting for swell dissipation over long distances has been cited as one of the likely dominant causes for overestimation of significant wave height (Ardhuin et al. 2009). Therefore, model predictions accounting for swell dissipation using the ST4 physics package of WWIII are compared to the same baseline model to quantify any improvements in model performance. Swell dissipation effects are not modeled directly with SWAN, but are investigated by inputting wave boundary forcing from the WWIII (ST4) model.
- Model comparison for large waves: The model predictions of WWIII and SWAN during extreme seas caused by storms are evaluated to investigate the limitations of WWIII and SWAN to predict large waves when using default model settings. This model case will serve as a baseline for developing calibration strategies to improve large wave predictions.

The present study details modeling methodologies and procedures, based on best practices, including model selection, establishing model boundary conditions, specifying the appropriate spatial and temporal resolution, analyzing model sensitivity, and documenting model performance. It provides met-ocean and other information about the common test bed selected for this study, along with justification for its selection. It defines the model domain, baseline test case, period of simulation, and the model data sources used for model inputs and model validation.

To provide independent review and guidance for the present study, a steering committee was formed. The committee was composed of several wave modeling experts (Drs. Tuba Özkan-Haller, Bryson Robertson, and Arun Chawla), a national laboratory representative conducting wave resource assessment

studies (Dr. Levi Kilcher), and a WEC industry representative with technical expertise in WEC technology research and development (R&D) (Dr. Tim Mundon). This committee provided valuable input during the modeling study planning process, provided guidance on model inputs and model setup, and reviewed preliminary results.

2.0 Model Test Bed Selection

The following criteria were used for the selection of the wave model test bed for the present study:

- The test bed includes areas with high resource potential based on the national wave energy resource assessment (EPRI 2011), as shown in Figure 2.1, which can be developed as viable commercial WEC projects.
- The met-ocean data at this test bed is in the vicinity of a viable commercial WEC location that has representative depth, involves high-quality wave measurements (e.g., wave direction measurements), and a reasonable POR of between 5 and 10 years.
- Information and data from previous studies at this test bed can be leveraged for this study.

Figure 2.1. Annual average wave power density (kW/m) around the US coast from national wave energy resource assessment (EPRI 2011).

Based on these criteria, a model test bed on the Central Oregon Coast (COC), approximately centered offshore of Newport, Oregon, was selected for this study. This test-bed site is delineated in Figure 2.2 along with locations of National Data Buoy Center (NDBC) observations. The COC test bed includes areas with large wave energy resource potential; wave power densities range between 35 and 50 kW/m (EPRI 2011). It also includes Tier 1 WEC test sites, as described by Dallman and Neary (2014), such as the Pacific Marine Energy Center's (PMEC) active North Energy Test Site (NETS), and planned South Energy Test Site (SETS).

The COC test bed included multiple met-ocean observations detailed in Table 2.1. Buoy data are accessible online at the CDIP and NDBC databases. Directional spectral wave observations from NDBC buoys and acoustic wave and current (AWAC) sensors could be used to evaluate model performance as

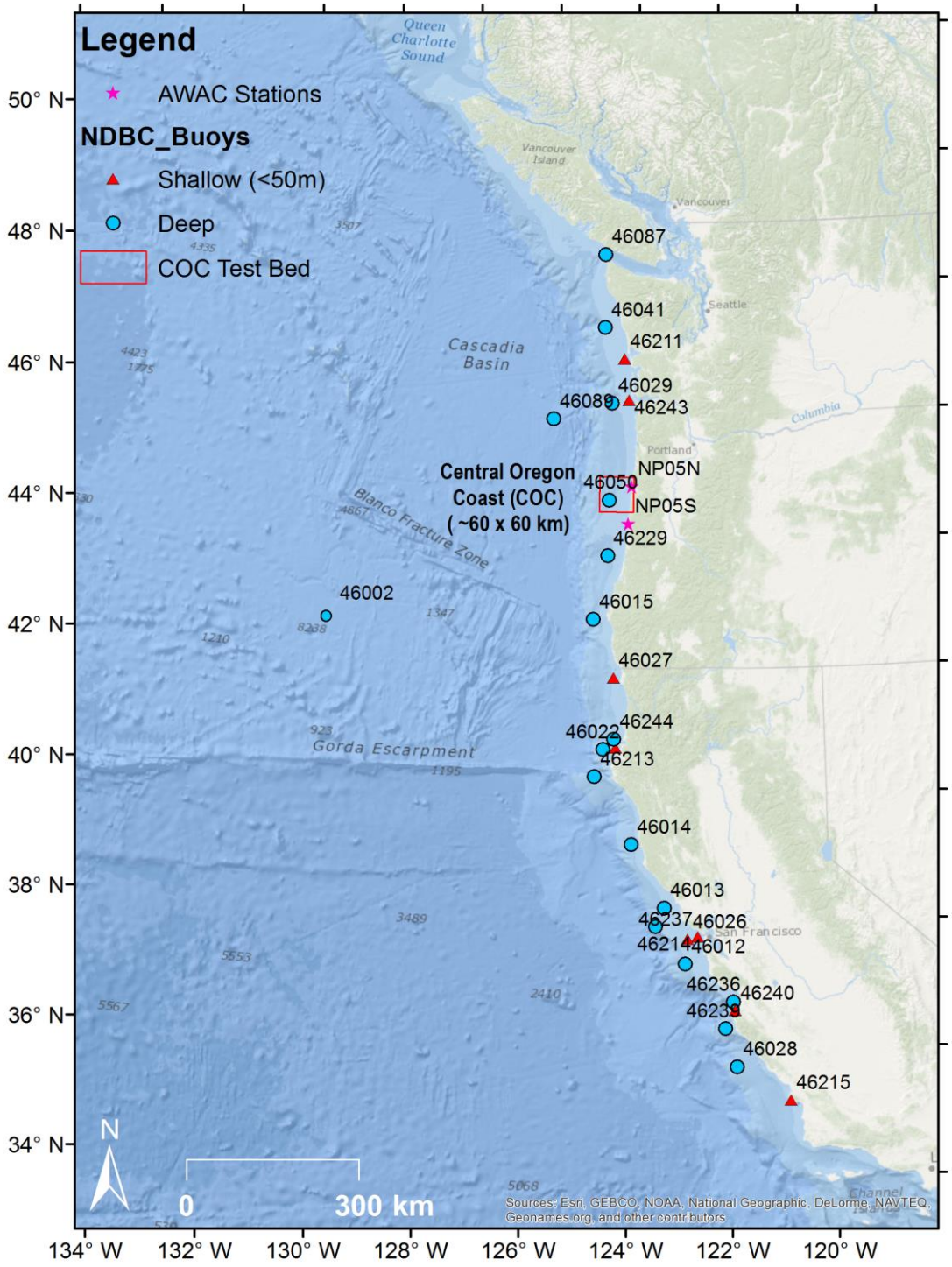

Figure 2.2. Location map showing NDBC/AWEC buoy locations at the selected model study test bed.

described in Methods, Section 3.3. The buoy measurements are located at depths where WEC deployments are likely, and of sufficiently long durations with PORs greater than 5 years. AWAC measurements are less than a year, and are at shallow depths (~10 m), but these measurements could be used in future studies to investigate model accuracy at very shallow depths. Wave direction data for NDBC 46050 are only available starting in March 2008. Wave direction data for calendar years 2009 and

2010 are complete, but some data are missing for 2011. For wind forcing data, Climate Forecast System Reanalysis (CFSR) (Saha et al. 2010) data are available from 1979 to 2010.

The test bed also includes or overlaps areas where previous wave model studies have been conducted (García-Medina et al. 2014; García-Medina et al. 2013; and Dallman and Neary 2014). The wave model study by Dallman and Neary (2014) used hindcast simulations to characterize the wave energy resources at PMEC's NETS, located in the COC test bed. Wave resource characterization of the NETS leveraged hindcast outputs from García-Medina et al. (2014).

In addition to the hindcast data set, Dallman and Neary (2014) used historical data from buoy NDBC 46050 to predict extreme sea states and representative spectra. Wind data were available from NDBC 46050 and a Coastal-Marine Automated Network (C-MAN) station, NWPO3, located just on-shore. To be consistent with the other sites in their study, CFSR winds were used.

Researchers at the Northwest National Marine Renewable Energy Center (NNMREC) produced a seven-year hindcast data set for the area offshore of Oregon (García-Medina et al. 2014) in order to complement the study of temporal and spatial variability in the wave resource over the Pacific Northwest region by Lenee-Bluhm et al. (2011). This data set was used to calculate statistics of interest for the wave resource characterization at NETS. The hindcast data at the grid point on the north side of NETS were analyzed. Although a 10-year hindcast would be preferred, García-Medina et al. (2014) showed that the probability density function (PDF) of significant wave height from their hindcast data compared to NDBC46029 buoy data were in agreement up to approximately the 7 m wave height.

Table 2.1. Wave observations within the COC study domain.

Instrument	CDIP139 / NDBC Station 46229	NP05N/NP05S/RP09	NDBC Station 46050 (Stonewall Bank)
Type	Waverider Buoy	AWAC Deployments	3-meter discus buoy
Measurements	-std. met. -spectral wave density -spectral wave direction	-spectral wave density -spectral wave direction	-std. met. -continuous wind -spectral wave density -spectral wave direction
Reported variables (Sampling interval)	-std. met: WVHT, DPD, APD, MWD, WTMP (30 min) -spectral wave density (cont.) -spectral wave direction(30 min)	1-Hz near-surface along-beam velocity (for three beams), 2-Hz acoustic surface height (from center beam), and1-Hz bottom pressure observations to resolve directional wave spectrum	-std. met: WDIR, WSPD, GST, WVHT, DPD, APD, PRES, ATMP WTMP (1 h) - cont. wind: WDIR, WSPD, GDR, GST, GTIME (10 min) -spectral wave density (cont.) -spectral wave direction (30 m)
Location	Umpqua offshore, OR	Newport, OR/ Newport, OR/ Offshore Reedsport, OR	20 nm (nautical miles, 1 nm = 1.852 km) directly west of Newport, 30 km west of NETS
Coordinates	43.767 N 124.549 W (43°46'0" N 124°32'58" W)	TBD	44.639 N 124.534 W (44°38'20" N -124°32'2" W) Note: 2009 buoy location at 44.6411N, 124.4997W
Depth	- depth: 182.9 m - temp depth: 0.46 m below msl	13 m/15 m/40 m	-depth: 128 m -air temp: 4 m above water -anemometer: 5 m above msl -barometer: msl -temp depth: 0.6 m below msl
Data Start	7/13/2006	7/23/2005, 6/15/2005, 9/18/2005	-Std Met: 11/16/1991 -Wind: 09/07/1997 -S. Wave Density: 01/01/1996 -S Wave Dir: 03/05/2008
Data End	present	9/22/2005, 7/13/2005, 12/2/2009	present
Period of Record	~8.5 yr	~2 months/~1 month/~2 months	-std met: ~23 yrs -contin winds: ~17 yrs -spect wave dens: ~19 yrs -spect wave dir: ~6.5 yrs
Data Location	NDBC/NOAA: http://www.ndbc.noaa.gov/station_page.php?station=46229	Oregon State University. García-Medina et al. 2013 and Kirincich et al. 2009	NDBC/NOAA: http://www.ndbc.noaa.gov/station_page.php?station=46050

3.0 Methods

3.1 Model Setup

The model setup for the wave modeling study consists of three important components: bathymetry creation, model grid generation, and imposition of model boundary conditions, as described below.

3.1.1 Model Bathymetry

The eastern Pacific Ocean coast has a narrow continental shelf and a deep outer-shelf basin. The model test bed, which corresponds to the local (L4) model domain, is located within the continental shelf (see Section 3.1.3 for a definition of the local model domain). Depths within the model domain range from zero to 602 m, with a mean depth of 165 m, and a standard deviation of 123 m.

Model bathymetry for the present study was created from the NOAA 3 arc-second (90 m) Coastal Relief Model for the inner shelf region (http://www.ngdc.noaa.gov/mgg/bathymetry/maps/area5.html), and the NOAA 1 arc-minute ETOPO1 Global Relief Model. The resolution of the Coastal Relief Model data set is sufficient for the inner shelf region because the local model grid resolution is ~200 m. High-resolution 1/3 arc-second bathymetry data were downloaded from http://www.ngdc.noaa.gov/dem/squareCellGrid/download/320, which covers the local model domain nearshore, and 3 arc-minute bathymetry data were downloaded from (http://www.ngdc.noaa.gov/mgg/coastal/crm.html) to cover the western portion of the local model grid shown in Figure 3.1. NOAA global relief (1 arc-minute ETOPO1, http://www.ngdc.noaa.gov/docucomp/page?xml=NOAA/NESDIS/NGDC/MGG/DEM/iso/xml/316.xml&view=getDataView&header=none) was used for areas in the western portion not covered by the 1/3 arc-second and 3 arc-second bathymetry data sets.

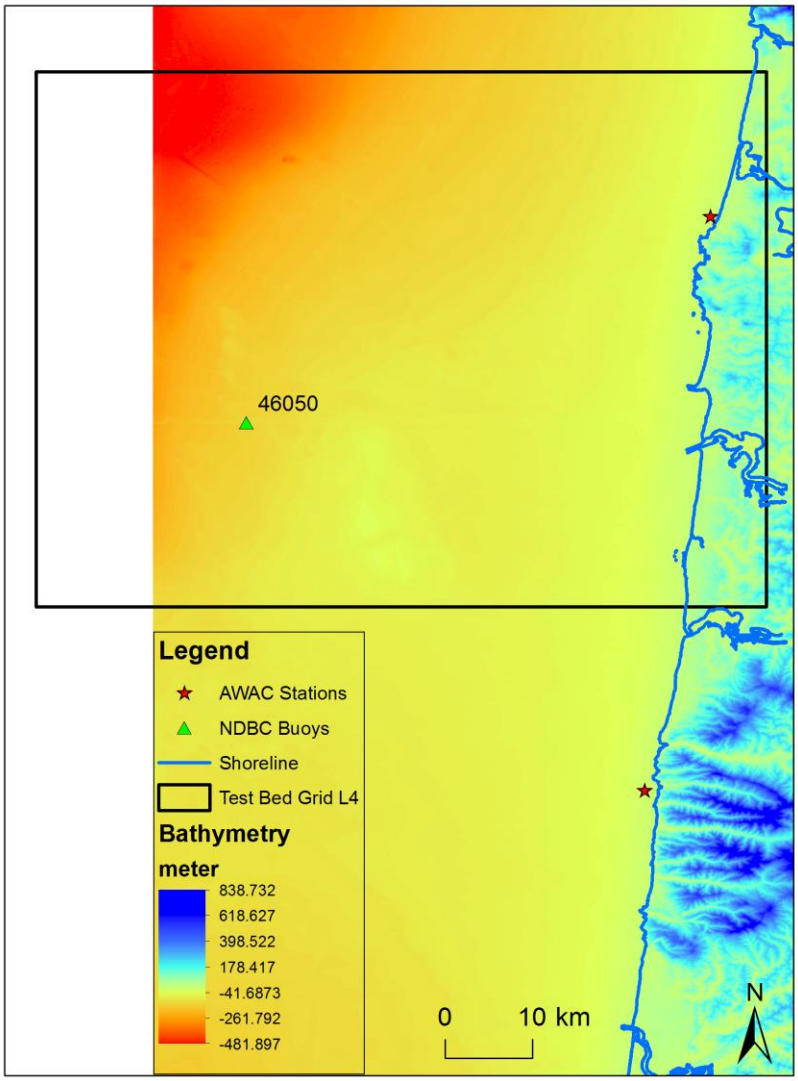

Figure 3.1. Local model domain with NOAA 1/3 arc bathymetry coverage and ocean observations.

3.1.2 Model Domains and Grids

3.1.3 Nested WWIII Grids

The present study employs a nested-grid modeling approach, consisting of three nested grids (L2–L4), within a global (L1) model grid, to generate open wave boundary conditions for the local model domain that delineates the model test bed. The boundaries and the bathymetries of the nested grids are shown in Figure 3.2 and Figure 3.3, respectively.

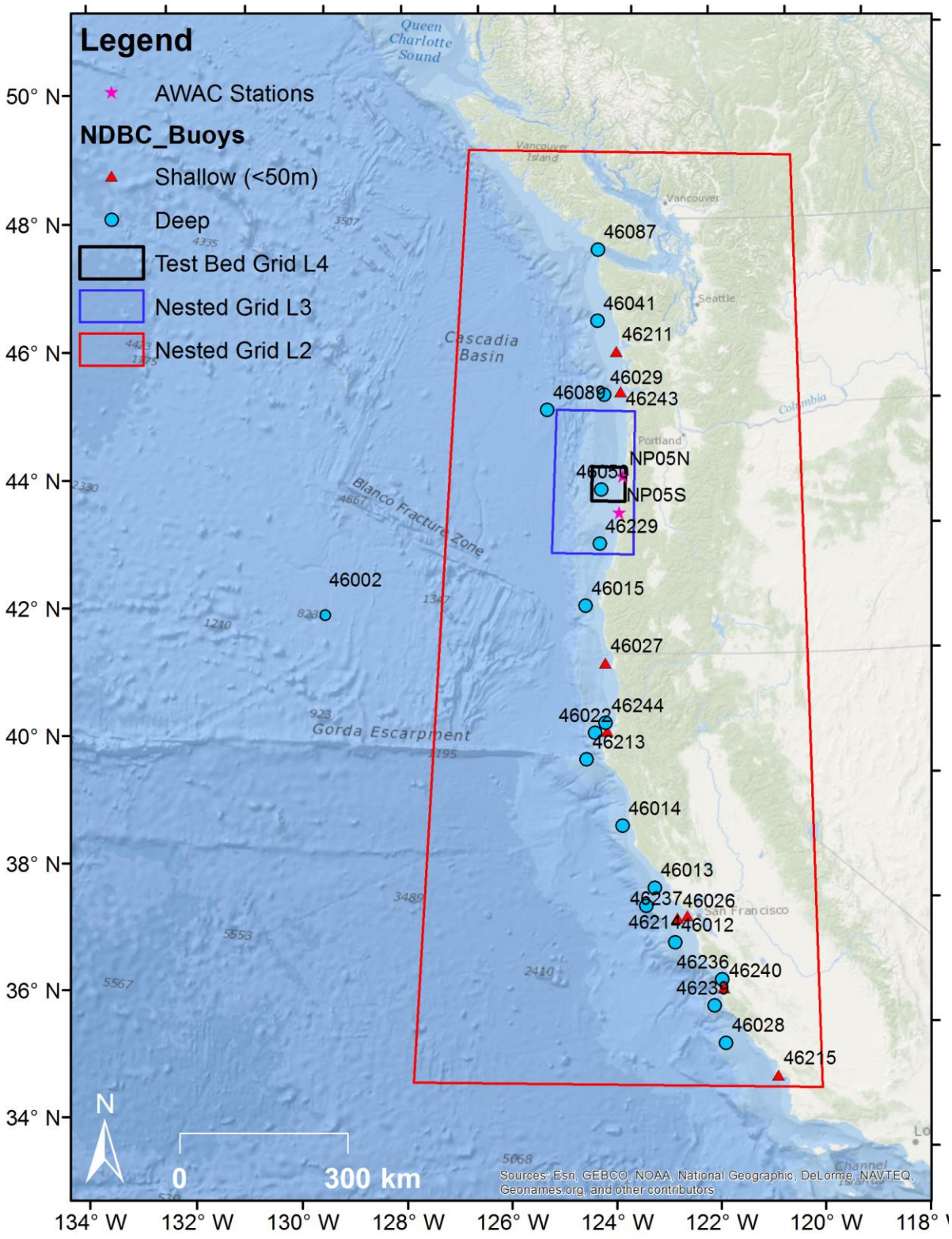

Figure 3.2. Boundaries of nested grids (L2–L4) for the modeling study.

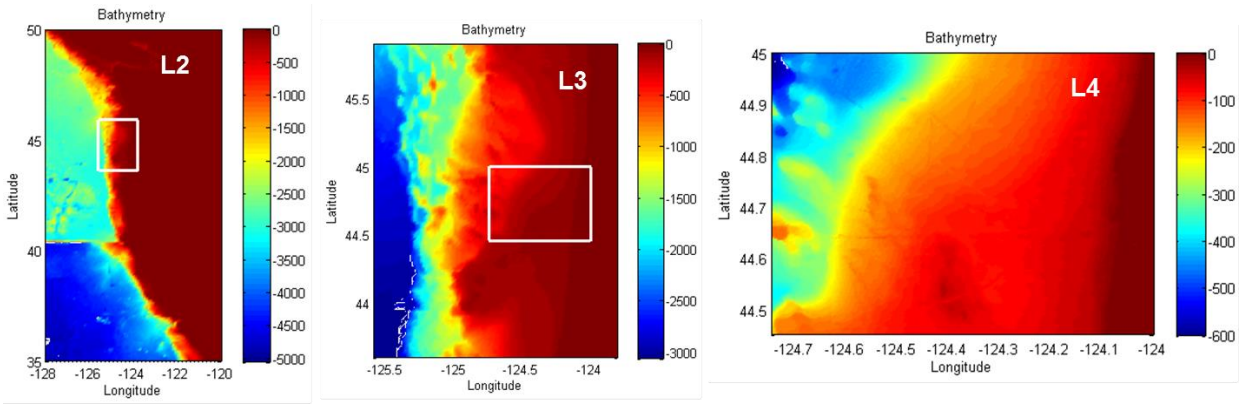

Figure 3.3. Bathymetries of nested grids (L2–L4).

The nested-grid scaling ratio (the ratio of the coarse-grid dimension to the fine-grid dimension) is set to a value of approximately five to six to maintain a smooth transition between model results along the nested-grid boundaries. This ratio results in the highest grid resolution of 265 m × 308 m for the test bed domain, and follows recommendations by the IEC TS 62600-101ED 1.0. The two intermediate regional nested grids have resolutions of 6 arc-minute and 1 arc-minute, respectively. For each of these grids, the domain coordinates (in latitude and longitude), spatial resolution (grid dimensions), and grid size (number of grid points) are summarized in Table 3.1. The resolution of the Global WWIII model domain is set at 0.5 degrees to correspond with the spatial resolution of the high-quality CFSR wind forcing data.

Table 3.1. Nested WWIII model grids.

Grid Name	Coverage	Resolution (long., lat.)	Grid size
Global Grid L1	77°S - 77°N	0.5° × 0.5° (30' × 30')	223,920
Nested Grid L2	35° - 50°N; 128° - 120°W	0.1° × 0.1° (6' × 6')	12,231
Nested Grid L3	43.6° - 45.9°N; 125.6°-123.8°W	1' × 1'	15,151
Test Bed Grid L4	44.45° - 45°N; 124.75° - 124°W	12"×10" (265m×308m)	44,974

The local model domain (L4) covers the NDBC 46050 buoy used in the present study's model validation. It also includes one shallow-water AWAC for future model evaluations (Figure 2.2). For the purpose of allowing future investigations of nearshore effects, e.g., shoaling, the domain must extend to the shoreline. These criteria require a model domain of approximately 60 km by 60 km at the COC site, which covers a region from 44.45°N to 45°N and from -124°W to -124.75°W (Figure 2.2). It should be noted, that this model domain size is significantly greater than the area that would be occupied by a 100-unit WEC array, which has been estimated to encompass approximately a 3 km by 3 km area with spacing between individual WEC devices of approximately 500 m (Neary et al. 2014).

3.1.4 Simulation Period

The calendar year 2009 was selected for the model simulation period based on the availability and completeness of wind forcing data, and met-ocean data for model validation at NDBC 46050. Spectral direction data at NDBC 46050 is available starting on March 5, 2008.

A full-year simulation allows for an evaluation of the seasonal effects on wave resource parameters; e.g., the strong seasonal variations of significant wave height shown in Figure 3.4 for NDBC 46050, with large waves occurring in winter, and relatively calm seas occurring during summer. The 99-percentile

significant wave height is 6.22 m based on the NDBC 46050 data. This significant wave height, which is equaled or exceeded about a dozen times, is used in the present study to delineate the minimum significant wave height threshold for investigating model performance for large waves, and it includes the first in a series of strong storms to hit the COC over a week period in mid-November, which is investigated in Section 4.4.

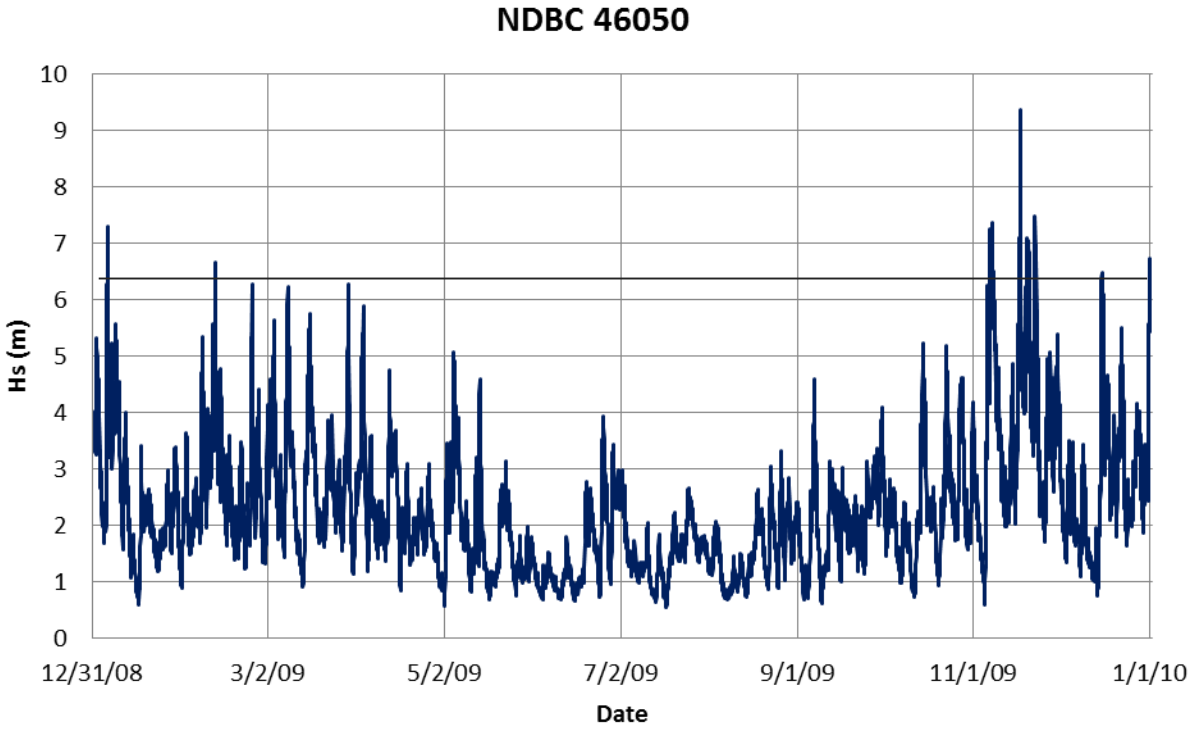

Figure 3.4. Significant wave height at NDBC 46050 for the 2009 calendar year. The redline indicates the 99-percentile significant wave height at 6.2 m.

3.1.5 Model Boundary Conditions

3.1.5.1 Wave Forcing

To drive the test bed (L4) grid models, three levels of nested grids with WWIII were implemented. The first level model used the NOAA/NCEP's global model with 0.5° grid resolution. The second level (L2) intermediate grid, with a resolution of six arc-minutes, was nested into the global model, and a third level (L3) intermediate grid, with a resolution of one arc-minute, was nested into the L3 grid. The L3 grid provides open wave boundary conditions for the fine-grid test-bed model (see Figure 3.2). Water bodies inside estuaries and bays along the coast were not included in the model domain.

3.1.5.2 Wind Forcing

Surface wind (technically it is U10 – wind at 10 m above mean sea level) is one of the important forcing mechanisms for wave propagation from the outer continental shelf to the inner shelf. To account for the wind-generated waves within the model domain, wind speed and direction were obtained from the 30-year hindcast simulations from the q `1 (Saha et al. 2010) and interpolated to the model grid points. The CFSR data set meets the minimum 1-hour temporal resolution requirements specified by the IEC TS

62600-101ED for design (Level 3) assessments. However, at 0.5-degree spatial resolution, which is 56 km latitude by 39 km longitude at 45-degrees latitude, it exceeds the minimum requirements for spatial resolution, which is 25 km for design, and 50 km for feasibility. Additional wind data are available from the Coupled Ocean/ Atmosphere Mesoscale Prediction System (COAMPS) model (Robertson et al. 2014), which can potentially be used in future sensitivity studies.

3.1.5.3 Water Level and Current Forcing

Although tidal currents can be strong along the west coast, especially in estuaries and bays along the Pacific Northwest coast, wave-current interaction induced by tides or ocean currents was not the focus of the present study. The IEC TS 62600-101ED 1.0 on Wave Resource Characterization recommends including ocean current data in wave models only if depth-averaged current speeds exceed 1.5 m/s. In general, this is unlikely for points of investigation during normal sea states because the model test bed is not close to any estuaries and bays with strong currents.

3.1.6 Baseline Model Configurations

The model configurations for the baseline simulations used in the present study involve WWIII, with the Source Term 2 (ST2) physics package, the SWAN nonstationary model (SWAN-NS), and the SWAN stationary model, (SWAN-S). In the ST2 physics package, the growth and dissipation are based on the physics by Tolman and Chalikov (1996). In the ST4 physics package, the Janssen (1989, 1991) growth and dissipation terms are used. All models use the same test-bed model grid with 12" × 10" (265 m × 308 m) grid resolution. Both models use default settings only; i.e., neither model is calibrated using a split-sample method. The baseline models use 29 frequency bins, 24 direction bins, a logarithmic increment factor of 1.1, and a minimum frequency of 0.035 Hz, which gives the maximum frequency of 0.505 Hz. This spectral resolution is similar to other regional model studies (e.g., Hanson et al. 2006), and meets the minimum requirements specified by IEC TS 62600-101ED (a minimum of 25 frequency components and 24 to 48 directional components, and a frequency range covering at least 0.04 to 0.5 Hz). The SWAN user's manual recommends a maximum frequency of ~1 Hz when modeling coastal areas, but the present study limits comparisons to buoy measurements where complex nearshore wave dynamics are not present.

The baseline model configuration meets the IEC TS 62600-101ED requirements for a "suitable numerical model," including boundary conditions defined by directional wave spectra, and all physical processes modeled with the exception of triad interaction, e.g., wind-wave growth, whitecapping, quadruplet interaction, wave breaking, and bottom friction. Because the present study only evaluates model skills by comparing with measurements at 128 m, triad interaction and bottom friction are negligible contributions.

To the extent possible, the source term models for SWAN were selected to agree with those in WWIII. Source term models for wave energy sources and sinks are summarized in Table 3.2. Common source/sink term models include those for linear wave growth (Cavaleri and Maltnotte-Rizzoli 1981), exponential wave growth (Janssen 1989, 1991), dissipation due to bottom friction (JONSWAP 1973), depth-induced breaking (Battjes and Janssen 1978), and nonlinear wave-wave of quadruplets (Hasselman et al. 1985). SWAN models dissipation due to whitecapping using the formulation by Komen et al. (1984), while WWIII (ST2) uses the turbulent boundary layer dissipation model described by Tolman and Chalikov (1996). As noted by Tolman et al. (2014), "… the wind-wave growth and dissipation are separate processes, but are interrelated, because the balance of these two source terms governs the integral growth characteristics of the wave model." Several combinations of these basic source terms are available in different physics packages of WWIII, as described by Tolman et al. (2014).

Table 3.2. Source term configurations in WWIII and SWAN.

Process	***WWIII***	***SWAN***	***Notes***
Linear wind growth	Cavaleri & Maltnotte-Rizzoli 1981	Cavaleri & Maltnotte-Rizzoli 1981	Only one model for linear term. Matches WWIII
Exponential wind growth	Janssen 1989, 1991	Janssen 1989, 1991	One of three models. Matches WWIII.
Whitecapping and turbulent boundary layer dissipation	Turbulent boundary layer dissipation only, Tolman & Chalikov 1996	Whitecap dissipation only, Komen et al. 1984	For WWIII (ST2), Model by Tolman & Chalikov 1996. For WWIII (ST4), Model by Ardhuin et al. 2010
Wave interaction	QUADS, Hasselmann et al. 1985	QUADS, Hasselmann et al. 1985	Default GEN3 ON. Matches WWIII
Breaking	Battjes & Janssen 1978	Battjes & Janssen 1978	Default ON. Matches WWIII
Friction	JONSWAP 1973	JONSWAP 1973	Default JONSWAP. Matches WWIII

Model time steps used in WWIII and SWAN are summarized in Table 3.3. For WWIII, each model grid requires four time steps, the global time step Δt_g, the spatial propagation time step Δt_{xy}, the intra-spectral propagation time step Δt_k, and the source term time step Δt_s (Tolman et al. 2014). The important time step that controls the model stability is the CFL time step Δt_{xy} for spatial propagation for the specific model grid resolution.

Table 3.3. Model run time steps for WWIII (L1 – L4 grids) and SWAN (L4 grid).

WW3 Nested Grid	Δt_g (s)	Δt_{xy} (s)	Δt_k (s)	Δt_s (s)
L1 (global)	3,600	480	1,800	30
L2	600	240	300	15
L3	100	45	50	15
L4 (test bed)	20	8	10	15
SWAN Grid	Δt_{xy} (s)	Input time (s)	Output time (s)	
L4 (test bed)	60	3,600	3,600	

Because the nonstationary SWAN model (SWAN-NS) uses an implicit scheme, the computational time step is not restricted by Courant stability criteria. However, the time step does affect the accuracy of the numerical solution. In the present study, a time step of 60 seconds was used for simulations. This time step is more than adequate to resolve the time variations of the computed wave field given the wind and open wave boundary forcing inputs are hourly. It also was shown not to affect the accuracy of the numerical solution. Sensitivity studies using smaller time steps, as low as 5 seconds, showed no improvement in the predicted wave parameters.

3.2 IEC TS 62600-101ED 1.0, Wave Resource Parameters

The six parameters recommended by the IEC TS 62600-101ED 1.0 for characterizing wave energy resources include omnidirectional wave power, significant wave height, energy period, spectral width, direction of maximum directionally resolved wave power, and directionality coefficient. All parameters are derived from the directional wave spectra that are represented by variance densities S_{ij}. Over each discrete frequency index i, and each discrete direction index j, Detailed descriptions of these parameters are provided by the technical specification, IEC TS 62600-101 (2015).

The omnidirectional wave power, J, is the sum of the contributions to energy flux from each of the components of the wave spectrum,

$$J = \rho g \sum_{i,j} c_{g,i} S_{ij} \Delta f_i \, \Delta\theta_j$$

where ρ is the density of sea water, g is the acceleration due to gravity, $c_{g,i}$ is the group velocity, Δf_i is the frequency bin width at each discrete frequency index i, and $\Delta\theta_i$ is the direction bin width at each discrete direction index j,

Directionally unresolved parameters are calculated from one-dimensional (unresolved) frequency variance densities using the equation

$$S_i = \sum_j S_{ij} \Delta\theta_j.$$

For the purpose of the present study the significant wave height is defined as the zeroth frequency the spectral moment as

$$H_s \sim H_{m0} = 4\sqrt{m_0}$$

where the moments of a variance spectrum are generally defined as

$$m_n = \sum_i f_i^n S_i \Delta f_i.$$

As noted by Tucker and Pitt (2001), this definition of significant wave height was used up until 1990 in the United Kingdom until it was defined as the average of the one-third highest zero-crossing waves by the International Association of Hydraulic Research (IAHR 1989). Both definitions give similar results if the distribution of the wave heights fit a Raleigh distribution

H_s is typically paired with the energy period, T_e, calculated as

$$T_e = \frac{m_{-1}}{m_0},$$

to define a wave climate's sea state. The energy period is the variance-weighted mean period of the directionally unresolved variance density spectrum. It is preferred over the peak period because because it is not sensitive to the spectral shape.

The spectral width, ϵ_0

$$\epsilon_0 = \sqrt{\frac{m_0 m_{-2}}{(m_{-1})^2} - 1},$$

is a measure of the spreading of energy along the wave spectrum. The directionally resolved wave power is the sum of the wave power at each direction θ

$$J_\theta = \rho g \sum_{i,j} c_{g,i} S_{ij} \Delta f_i \, \Delta\theta_j cos(\theta - \theta_j)\delta$$
$$\begin{cases} \delta = 1, & cos(\theta - \theta_j) \geq 0 \\ \delta = 0, & cos(\theta - \theta_j) < 0 \end{cases}$$

where J_θ is the directionally resolved wave power in direction θ. The maximum time-averaged wave power propagating in a single direction, J_{θ_J}, is the maximum value of J_θ. The corresponding direction, θ_J, is the direction of maximum directionally resolved wave power and describes the characteristic direction of the sea state.

The directionality coefficient, d, is the ratio of maximum directionally resolved wave power to the omnidirectional wave power,

$$d = \frac{J_{\theta_{jmax}}}{J},$$

which is a characteristic measure of directional spreading of wave power (i.e., larger values approaching unity signify narrow directional spread).

In the present study, each of these parameters is calculated hourly from directional wave spectra predicted by numerical models and buoy measurements.

3.3 Model Performance Metrics

For evaluation of model performance, the six IEC TS 62600-101ED 1.0 parameters generated from model hindcasts over the 2009 calendar year are compared to those from point measurements from NDBC 46050 (Stonewall Bank, 20 nautical miles west of Newport, Oregon). For each of these IEC TS 62600-101ED 1.0 parameters, the following model performance metrics are computed to quantify the discrepancies between the predicted values derived by model hindcasts and those derived by the NDBC 46050 point measurements. All of these metrics represent an average estimate of the difference between predicted values and measured ones over a defined period of simulation.

The root-mean-square-error (*RMSE*), *aka* root-mean-square-deviation (*RMSD*), is defined as

$$RMSE = \sqrt{\frac{\sum_{i=1}^{N}(P_i - M_i)^2}{N}}$$

where N is the number of observations, M_i is the measured value, and P_i is the predicted value.

RMSE represents the sample standard deviation of the differences between predicted values and measured values.

The scatter index (*SI*) is the RMSE normalized by the average of all measured values over the value of comparison, where

$$SI = \frac{RMSE}{\bar{M}},$$

where the overbar indicates the mean of the measured values.

Model bias, which represents the average difference between the predicted and measured value, is defined as

$$Bias = \frac{1}{N}\sum_{i=1}^{N}(P_i - M_i),$$

Percentage bias, which is defined as

$$Bias(\%) = \frac{\sum_{i=1}^{N} P_i - \sum_{i=1}^{N} M_i}{\sum_{i=1}^{N} M_i} \cdot 100$$

is also commonly used to normalize bias.

The linear correlation coefficient, R, is defined as

$$R = \frac{\sum_{i=1}^{N}(M_i - \bar{M})(P_i - \bar{P})}{\sqrt{\left(\sum_{i=1}^{N}(M_i - \bar{M})^2\right)\left(\sum_{i=1}^{N}(P_i - \bar{P})^2\right)}}$$

and is a measure of the strength of the linear relationship between the predicted and measured values.

4.0 Results

4.1 Baseline Simulations

Results of model performance for the baseline simulations in the model test bed are presented in the following sections, where model performance, *aka* model skill, is defined as the ability of the model to simulate values of the six wave resource parameters derived from measurements at NDBC 46050. Model skill is analyzed by comparing the time-series plots of these wave resource parameters, quantile (Q-Q) plots, and performance metrics as defined in Section 3.3. Before analyzing model performance in the test bed, however, the nested WWIII modeling results are analyzed to determine that model nesting was implemented successfully.

Maps showing the spatial distribution of significant wave height, based on WWIII model simulations, are plotted to demonstrate the successful implementation of the nested-grid approach. Smooth distributions of the significant wave height, specifically the absence of any discontinuities across the four nested-grid boundaries, demonstrates the successful implementation of the nested-grid approach. Figure 4.1 shows the spatial distribution of significant wave height simulated by the global WWIII model between July 2 and November 7, 2009. In the US west coast region, significant wave heights in July are generally less than 5 m, and much smaller than those observed in November; especially along the Washington and Oregon Coasts. Figure 4.2 shows the significant wave height distribution in a magnified area of the west coast, including offshore of Vancouver Island, Canada. The region shown in Figure 4.2 covers areas from the global grid (L1) to the test-bed grid (L4).

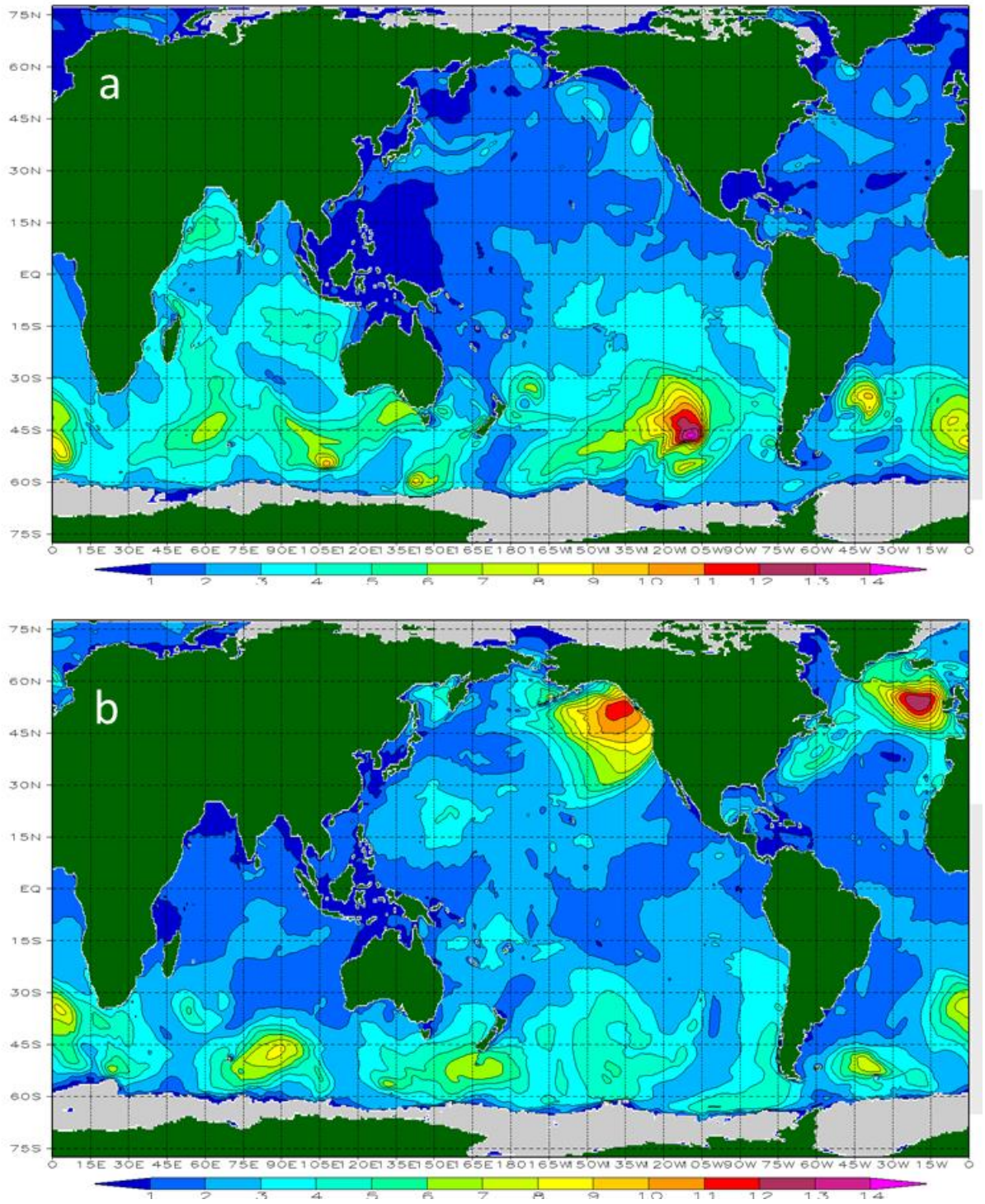

Figure 4.1. Global distribution of significant wave height simulated by WWIII for July 2 and November 7, 2009.

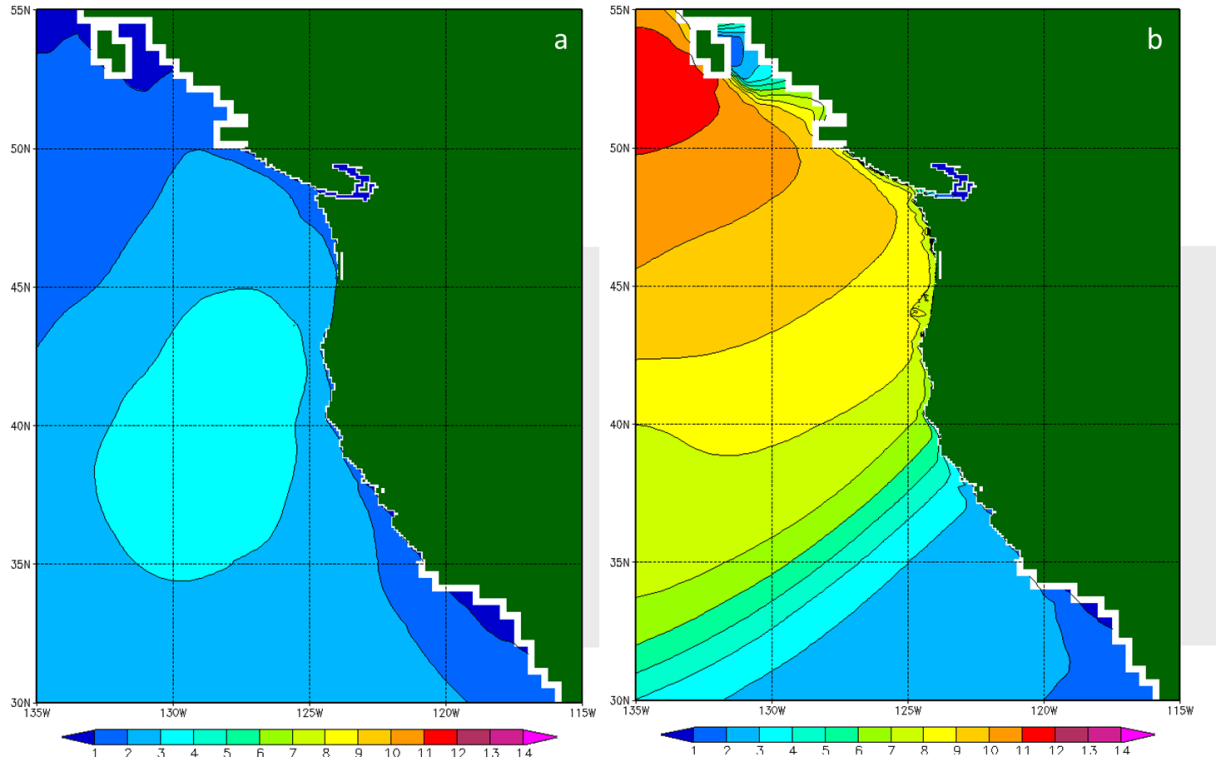

Figure 4.2. Regional distribution of significant wave height simulated by WWII with nested grid (L1 – L4) for July 2 and November 7, 2009.

4.1.1 Model Test Bed – Baseline Simulations

A comparison of the significant wave height time series predicted using WWIII in the present study with those from NOAA's WWIII model with a grid resolution of 4 arc-minutes, and NDBC 46050 measurements is shown in Figure 4.3. Overall, the test-bed WWIII results are very similar to those from the NOAA WWIII 4' x 4' hindcast simulations, especially during the summer months when waves are small. However, there are noticeable improvements due to the increased grid resolution in predicting the peaks in the wave height time series and large waves. This improvement, albeit for only the parameter of wave height, provides confidence that the test-bed WWIII model settings for this baseline case are properly implemented. The predicted time series for significant wave height using the SWAN-NS model is in good agreement with that using the WWIII model (Figure 4.4), and likewise provides confidence in the SWAN model settings.

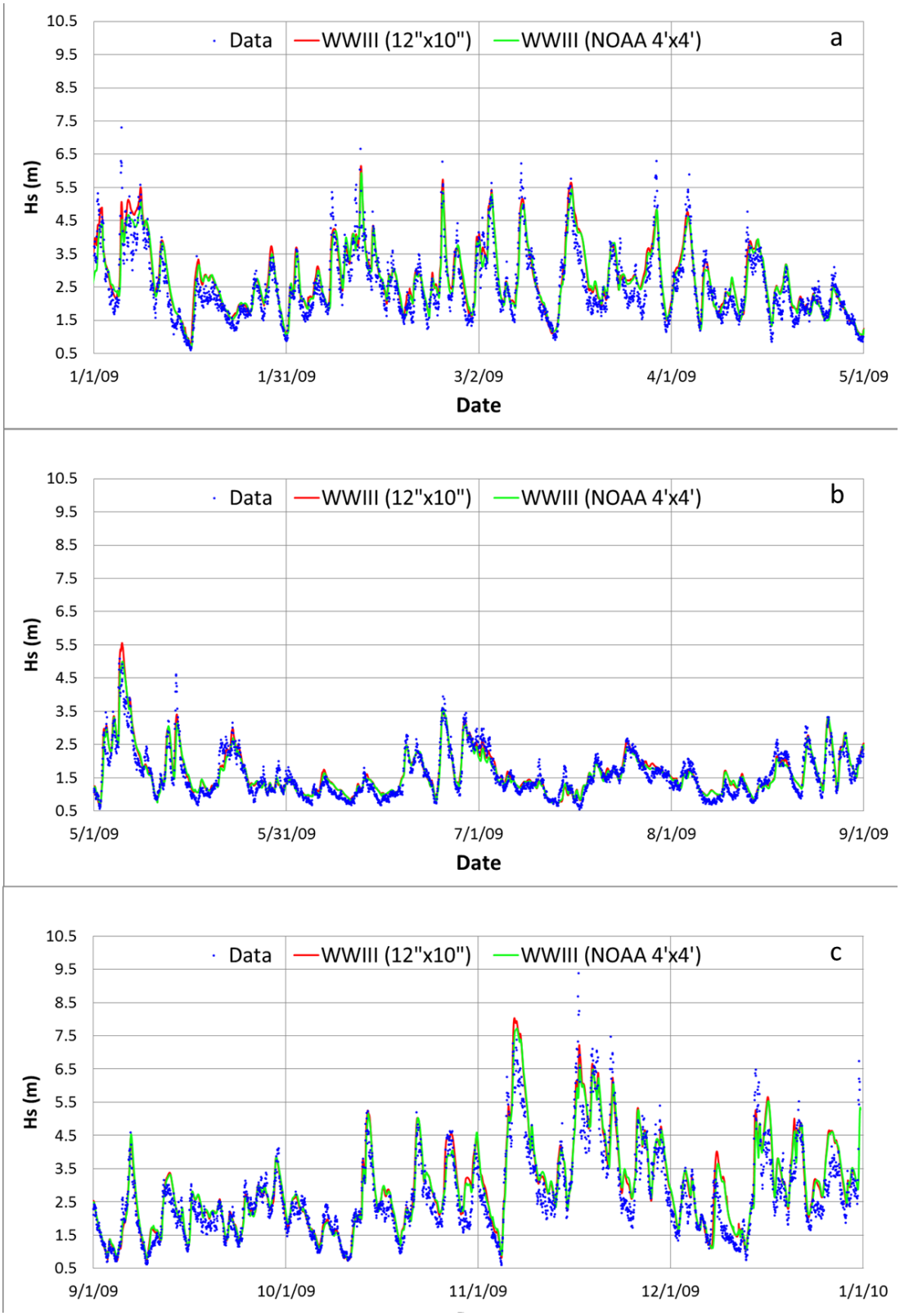

Figure 4.3. Comparison of significant wave height derived from the test-bed WWIII (red), with those derived from NOAA's 4' x 4' WWIII (green) and from buoy measurements (blue dots) for a) January – April 2009; b) May – August 2009; c) September – December 2009.

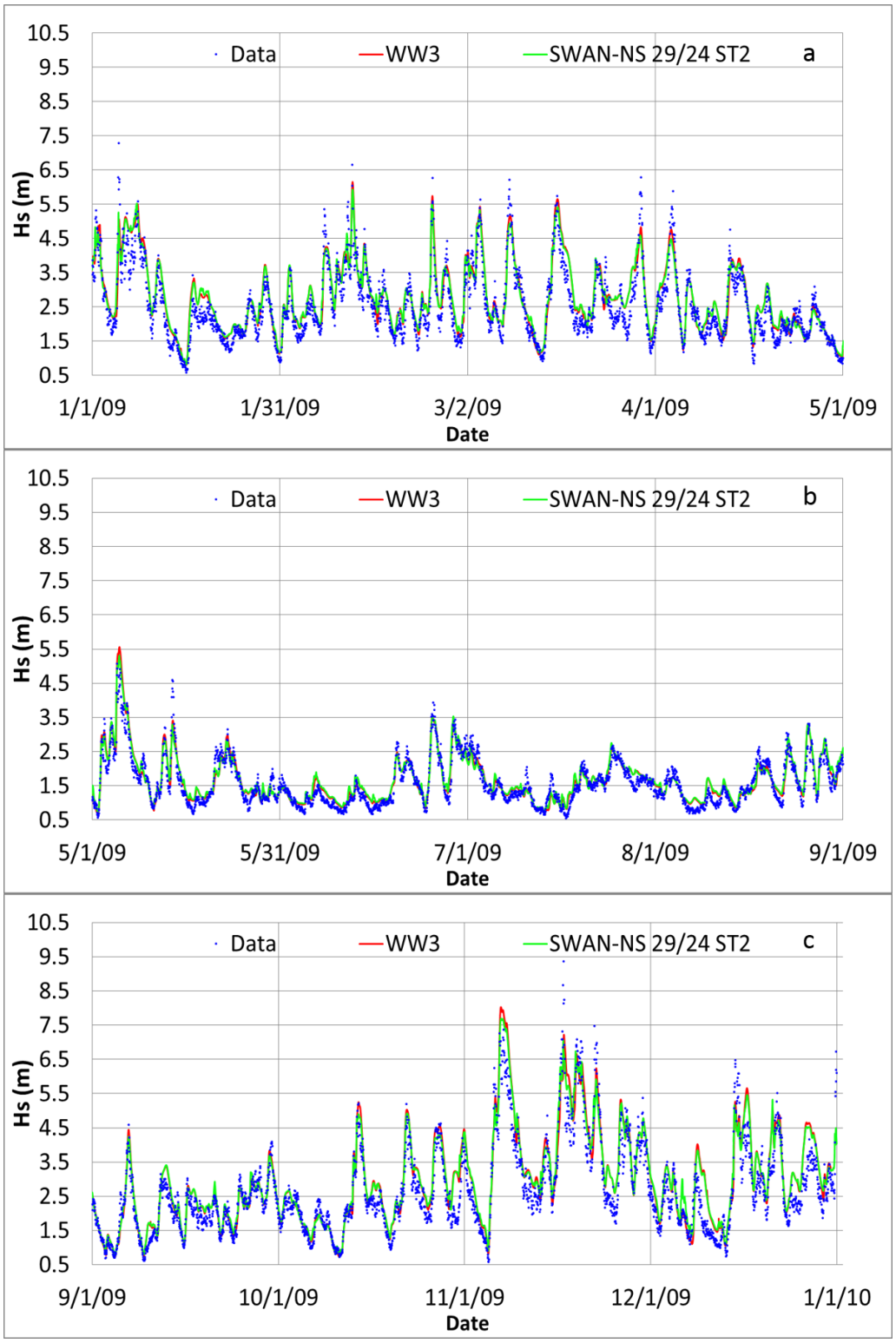

Figure 4.4. Comparison of significant wave height derived from models and derived from buoy measurements for a) January – April 2009, b) May – August 2009, c) September – December 2009.

Q-Q plots for H_s are shown in Figure 4.5 for both models. These plots show excellent correlation between predictions and measurements with R = 0.94 for both models, but the strength of the correlation depends on the magnitude of H_s. More scatter is observed for large waves (H_s > 6 m), which indicates that model skill for predicting measured H_s associated with extreme seas is not as good as for normal seas. These results are consistent with other wave modeling studies (e.g., García-Medina et al. 2014), and show the challenge of modeling large waves associated with extreme sea states. While predicting measured H_s for extreme seas is not as important for characterizing the energy resource, it is important for determining wave loads for WEC design.

Detailed results for baseline model test cases are provided in Appendices: Appendix A includes time-series plots for all six IEC parameters. As with H_s, these plots indicate that parameters derived by the models are in good agreement with those derived from the measurements. Appendix B includes Q-Q plots for all six IEC parameters with R values. Q-Q plots for T_e and J, also show excellent correlation between predictions and measurements. Plots for T_e do not exhibit the heteroscedastic behavior observed for H_s, but this behavior is even more pronounced for J compared to H_s, because J is proportional to H_s squared.

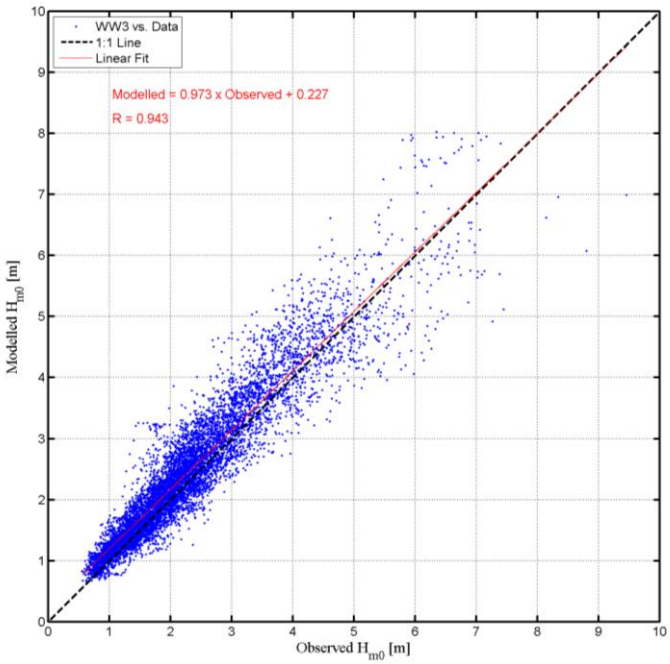

(a)

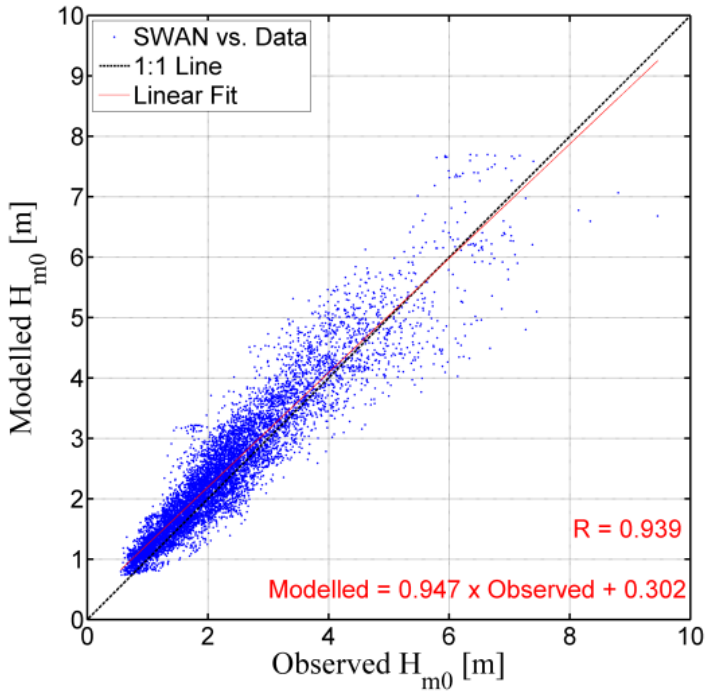

(b)

Figure 4.5. Scatter plots of significant wave height, 2009: a) WWIII and b) SWAN.

The computed performance metrics for each of the six IEC parameters are shown in Table 4.1 for the baseline test cases. The values for these metrics indicate that the model skills for all three model runs are

similar; and in good agreement to the observations at NDBC 46050. Correlation coefficients for J, H_s and T_e are all above 0.9.

Table 4.1. Performance metrics for baseline test cases.

Parameter	Model	RMSE	SI	Bias	R
J (kW/m)	WWIII	20.0	0.64	6.1	0.91
	SWAN	20.0	0.63	6.5	0.91
	SWAN-NS	19.0	0.62	6.3	0.91
H_s (m)	WWIII	0.42	0.19	0.16	0.94
	SWAN	0.45	0.20	0.19	0.94
	SWAN-NS	0.44	0.20	0.18	0.94
T_e (s)	WWIII	0.98	0.11	0.50	0.90
	SWAN	0.96	0.11	0.51	0.91
	SWAN-NS	0.95	0.11	0.52	0.91
ϵ_0 (-)	WWIII	0.07	0.20	0.01	0.68
	SWAN	0.07	0.20	0.00	0.71
	SWAN-NS	0.06	0.19	0.00	0.72
θ (degrees)	WWIII	22.87	0.08	-6.87	0.74
	SWAN	22.62	0.08	-6.65	0.74
	SWAN-NS	22.24	0.08	-6.62	0.75
d_θ (-)	WWIII	0.10	0.13	0.05	0.48
	SWAN	0.10	0.12	0.04	0.55
	SWAN-NS	0.10	0.12	0.04	0.55

The errors statistics for the baseline model runs are similar to those in other previous studies in the region, indicating all three models performed well and model results are in good agreement to the observations at NDBC 46050. In particular, the RMSEs for J_{omni}, H_s and T_e are about 20.0 (kW/m), 0.42-0.45 m and below one second, respectively. The linear correlation coefficients for J_{omni}, H_s and T_e are all above 0.9. Predicted H_s has a bias towards over-prediction of measured values by 0.2 m (8%) by SWAN compared to 0.5 m (6%) for WWIII. The RMSE is less than 0.5 m with an SI of 0.20. Although model performance is almost the same for all models, WWIII, exhibits the best model skill for H_s prediction followed by SWAN-NS and SWAN. Model skill for T_e prediction is slightly better than for H_s. The predicted T_e has a bias towards over-prediction of measured values by ~0.5 s. Model skill for J prediction is less than for H_s and T_e because it combines energy and frequency parameters in its calculation. Like many other wave modeling studies, the models in the present study also show bias towards over-prediction of measured values by ~6 kW/m (~20%). The predicted ϵ_0 exhibits virtually no bias. However, predicted ϵ_0 is not as well correlated with measured values in the Q-Q plots compared to J, H_s, and T_e with R~0.7. The predicted θ has a bias towards under-prediction by less than 5 degrees. Bias error for d_θ is small, but with an R~0.5.

The small differences between the WWIII and SWAN-NS predictions are expected due to several factors. First, the WWIII (ST2) model's open wave boundary forcing is two-way nested, while the SWAN models are only one-way nested. Second, the WWIII (ST2) model used a third-order accurate scheme compared

to second-order accurate schemes employed by the SWAN-NS and SWAN-S models. Third, a whitecap dissipation model is used by SWAN, while a turbulent boundary layer dissipation model is used in WWIII, as noted in Table 3.3.

4.1.2 Potential Model Error Sources

Model errors can be caused by several factors, including the accuracy of bathymetry and wind forcing. Comparisons of simulated and observed significant wave heights show that the models tend to over-predict wave height in low wave energy conditions (summer) and under-predict wave height under high wave energy conditions (winter month) (Figure 4.3 and Figure 4.4). To evaluate the wind forcing used in the study, NCEP CFSR wind is compared to observed wind at NDBC 46027 and NDBC 46026 (Figure 4.6) and NDBC 46002 (Figure 4.7). The location of these buoy observations is shown in Figure 2.2. At two nearshore locations, NDBC 46027 and NDBC 46026, this comparison shows that the CFSR wind is over-predicted in low wind conditions and under-predicted in high wind conditions. This is consistent with the model bias observed in the simulated significant wave height and suggests that, improving wind forcing should improve model prediction under both low and high wave conditions. However, at NDBC 46002, which is located offshore (Figure 2.2), the CFSR wind matched the observed data quite well (Figure 4.7).

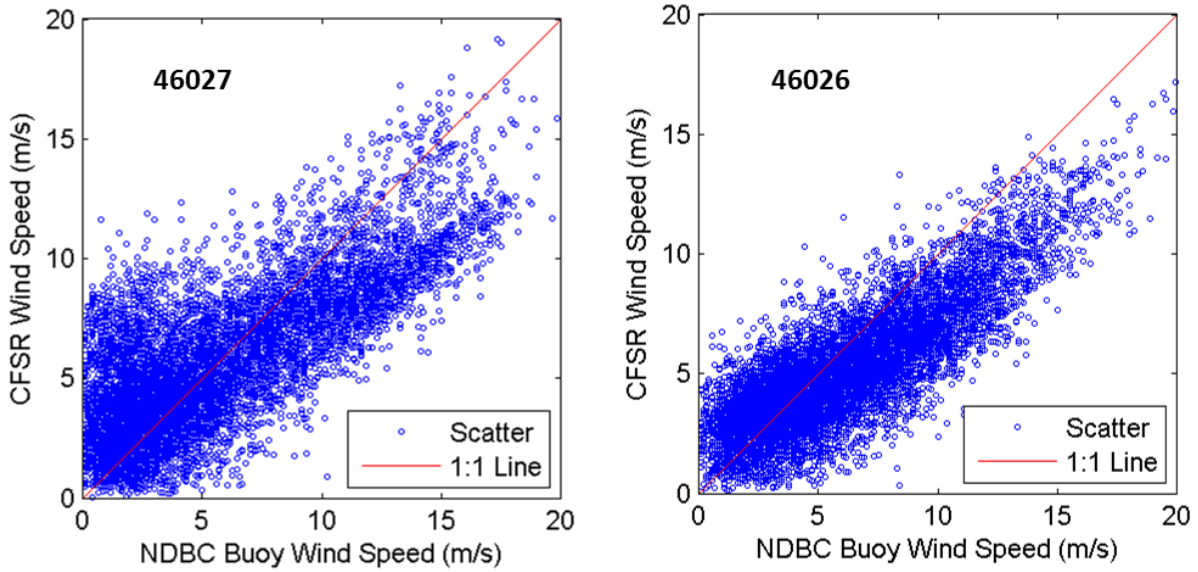

Figure 4.6. Comparison of CFSR wind to observed wind data at nearshore NDBC 46027 and NDBC 46026.

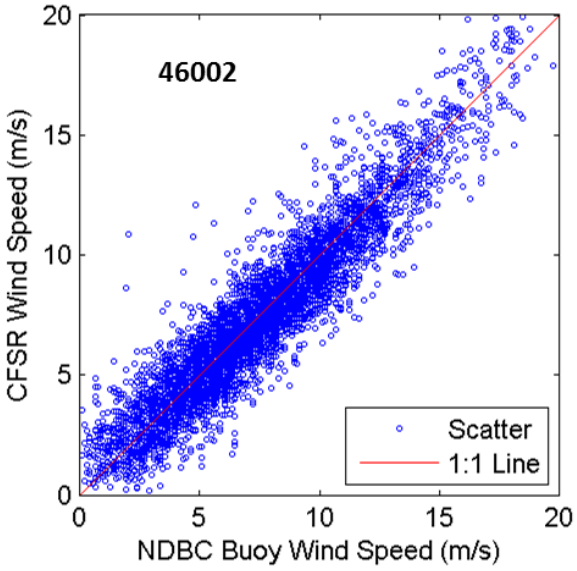

Figure 4.7. Comparison of CFSR wind to observed wind data at Buoy 46002 in the open ocean.

4.2 Spectral Resolution

A high spectral resolution, both in frequency and direction, is important to accurately model the advection of energy from swell over long distances. In particular, complex geometry and bathymetry in shallow-water regions will alter the frequency-directional characteristic of incoming waves. However, increase of spectral resolution in frequency and direction will also proportionally increase the computational time. Therefore, it is useful to assess the balance of model prediction accuracy vs. computational cost. Sensitivity model runs were conducted by varying the number of frequency and direction bins and comparing them to the baseline case with the fine-grid resolution model domain. Another two related parameters are the predefined directional sector within which waves travel shoreward and a frequency band with fixed low-frequency and high-frequency cutoffs. Narrowing the directional section and frequency band and maintaining the number of frequency and direction bins may increase model accuracy and computational efficiency.

The high spectral resolution sensitivity runs were set to match NOAA's WWIII operational forecast model settings, with the number of frequency bins set to 50, and the number of direction bins set to 36 (10 degrees). With a 1.07 increment factor, and a minimum frequency of 0.035, the maximum frequency is nearly 1 Hz at 0.96 Hz.

A comparison of the predicted significant wave height time series from the WWIII model with finer spectral resolution results from the baseline model, and observations at NDBC Buoy 46050, shows that increasing the spectral resolution, almost doubling the number of frequency bins, and increasing the direction bins by 50 percent provides no improvement in WWIII model skill (predicting wave resource parameters). Model insensitivity to spectral resolution was likely due to the large depth (128 m), and the absence of any bathymetric or geometric features at the point of comparison. Detailed results for the high spectral resolution WWIII simulations are provided in Appendices: Appendix A, time-series plots for all six IEC parameters; Appendix B, Q-Q plots; and Appendix C, performance metric summary tables.

Similar results were found in SWAN-NS and SWAN-S simulations; although these model sensitivity studies were limited to two 1-month simulation periods, one for the month of July and the other for the month of November. A comparison of significant wave height time series predicted with the finer spectral resolution SWAN-NS model and the baseline SWAN-NS model is shown in Figure 4.8 to illustrate the negligible effect of increased spectral resolution on model performance exhibited for all models. For all IEC TS 62600-101ED 1.0 parameters, except d_θ, the RMSE, PE, and SI increase slightly compared to the baseline case. Bias decreases slightly for most parameters in November, and increases slightly in July; but changes are marginal for both months.

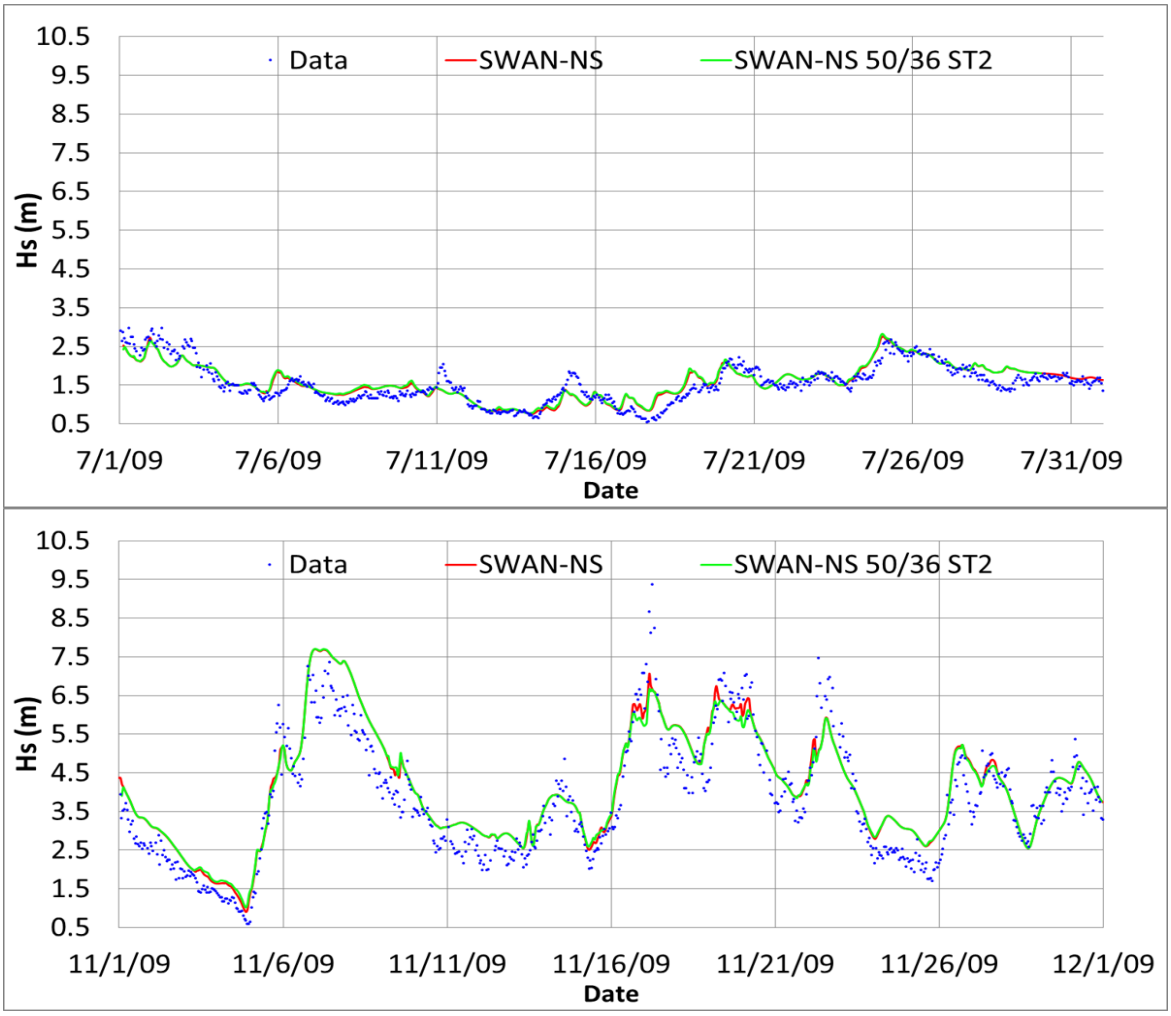

Figure 4.8. Sensitivity to increased spectral resolution SWAN-NS.

4.3 Swell Dissipation Effects

Swell dissipation effects are investigated with the nested-grid WWIII models using the ST4 package of WWIII, with default settings as described by Ardhuin et al. (2010). Model predictions accounting for swell dissipation were compared to the baseline case using the ST2 physics package with default settings as described by Tolman and Chalikov (1996), as well as NDBC buoy data, to quantify any improvements to model performance. The ST4 package includes not only swell dissipation effects, but also different growth and wave dissipation packages.

A comparison of significant wave height time series generated from the WWIII (ST4) and SWAN (ST4) model test cases with those generated from baseline test cases show mixed results (Figure 4.9 – Figure 4.11). Accounting for swell dissipation improves predictions of significant wave height compared to the baseline model that does not include these physics, but predictions of energy period are not as good. Although, differences in H_s prediction between these two test cases are generally marginal over most of the 2009 period of simulation, the ST4 model skill at predicting large H_s is noteworthy; particularly for

the periods where high seas due to severe storms occur in mid-November and early January (see Figure 4.11). Predictions of omnidirectional wave power density are also improved.

Model skills for predicting H_s improve by modeling swell dissipation; this supports claims by Ardhuin et al. (2009) that accounting for swell dissipation reduces the overestimation of significant wave height. RMSE, PE, and SI are reduced only marginally, but observed reductions in bias towards over-prediction of measured values are reduced by half, ~0.1 m (5%). Conversely, model skills for predicting T_e are slightly reduced. PE slightly increases from ~12%, for the baseline model, to ~15%. Bias towards over-prediction of measured values increases from ~0.5 s to ~0.8 s. Most noteworthy, the model skills for J prediction generally show significant improvement. Although PE increases to ~70% compared to ~60% for the baseline model, bias is reduced by almost half; e.g., 3.32 kW/m (10%) compared to 6.30 kW/m (20%) for the SWAN-NS baseline model. Model skills in predicting the remaining parameters, ϵ_0 , θ, and d_θ, are only slightly different than the baseline models, exhibiting insignificant changes in RMSE, bias, and R, and only small increases in PE.

Detailed results are provided in Appendices: Appendix A, time-series plots for all six IEC TS 62600-101ED 1.0 parameters; Appendix B, Q-Q plots; and Appendix C, performance metric summary tables.

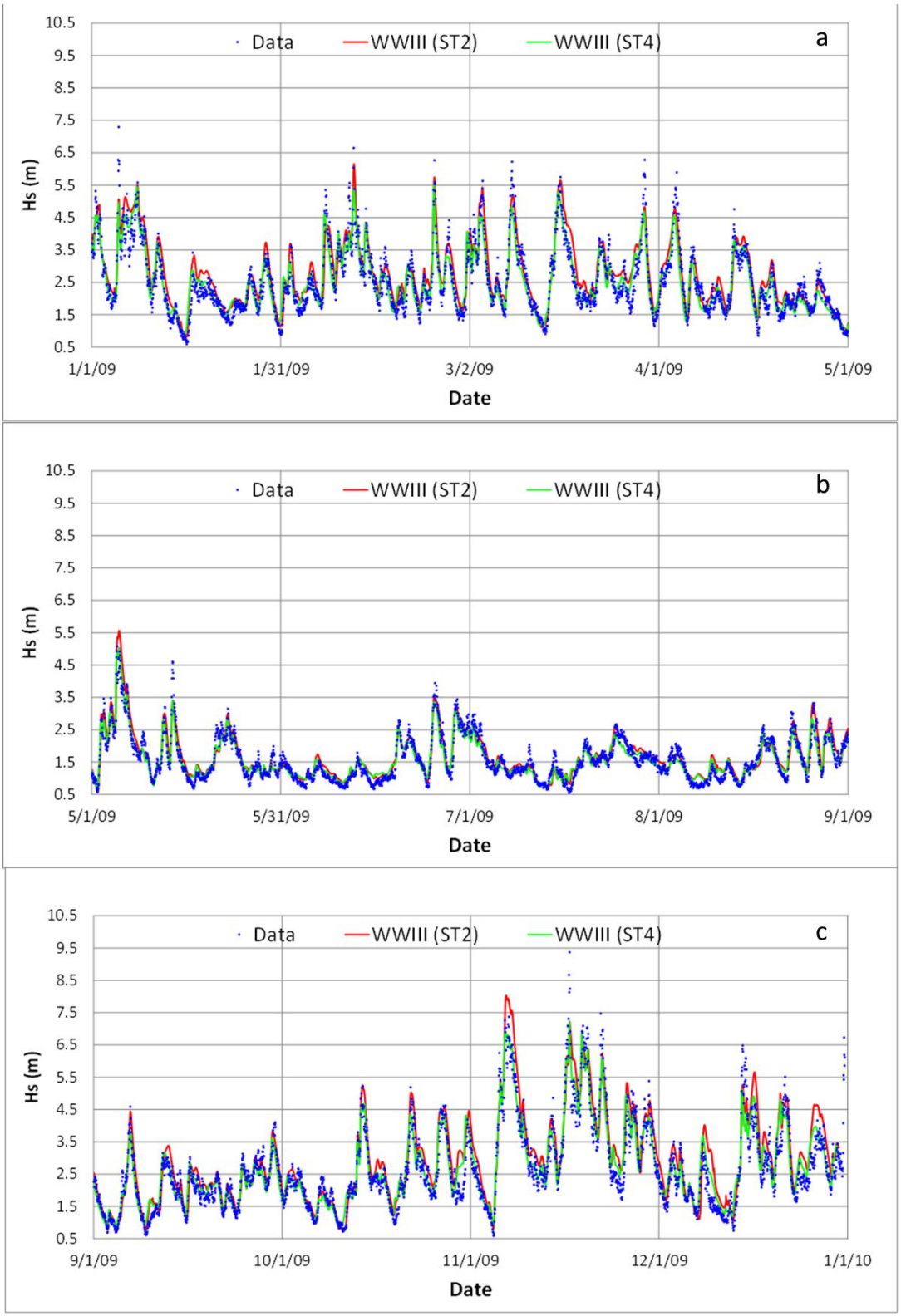

Figure 4.9. Comparison of significant wave heights from WWIII-ST2 (red), WWIII-ST4 (green), and buoy measurements (blue dots) for a) January – April 2009, b) May – August 2009, c) September – December 2009.

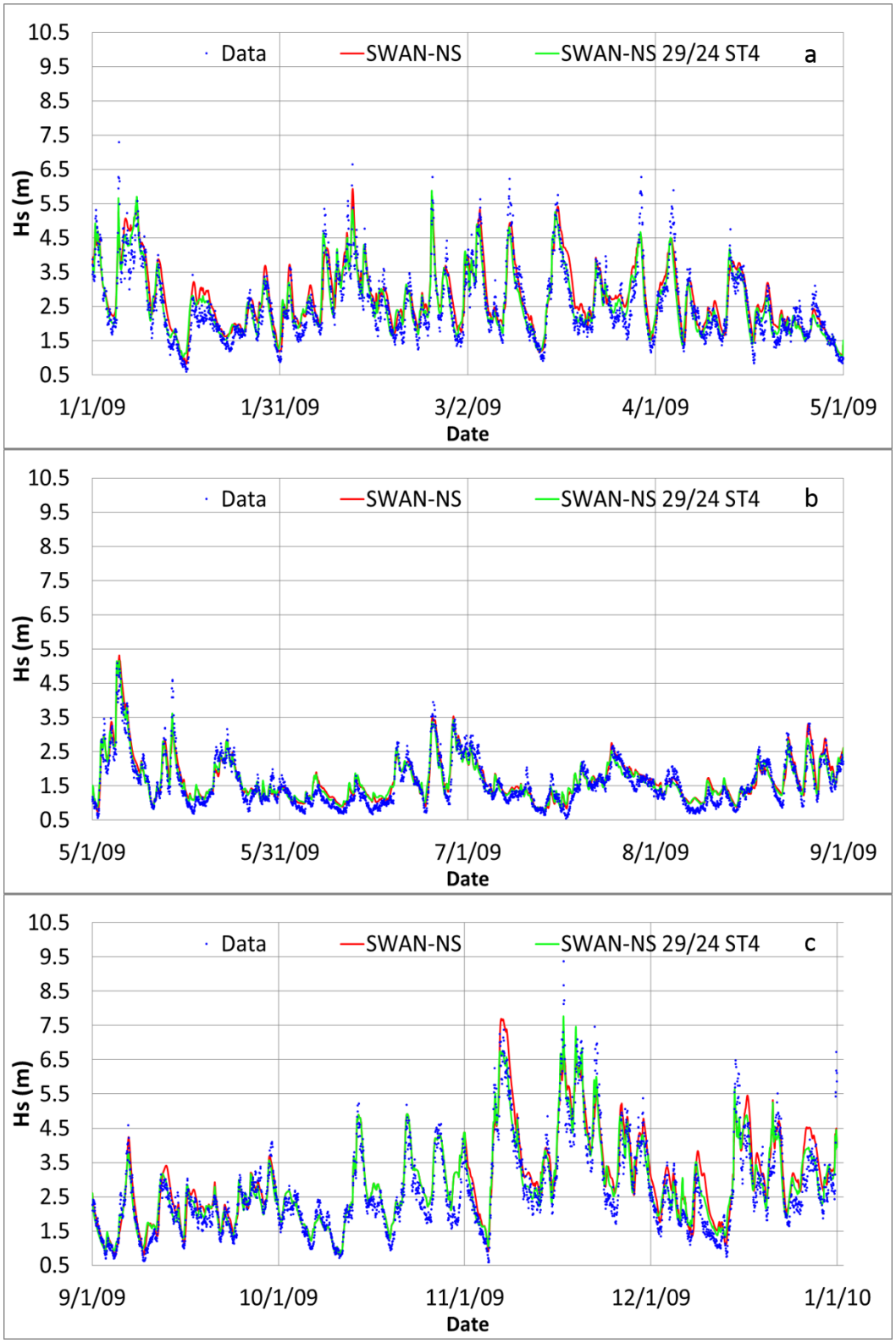

Figure 4.10. Sensitivity to swell dissipation, ST4 SWAN-NS.

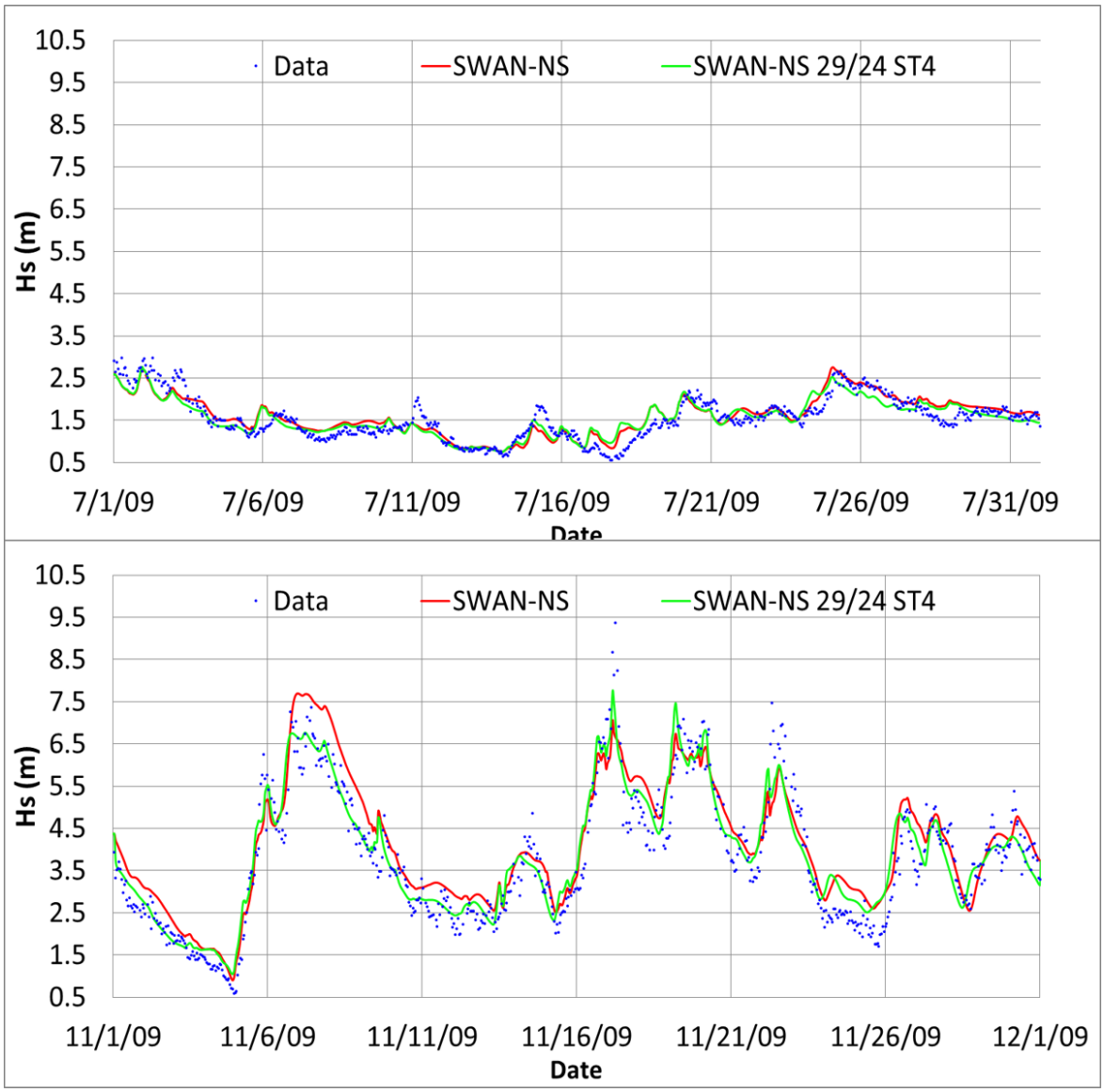

Figure 4.11. Sensitivity to swell dissipation, July and November 2009, ST4 SWAN-NS.

4.4 Large Waves

Extreme sea states provide critical information needed to assess the risks of deploying a WEC at a test site and to design a WEC to survive wave loads associated with extreme sea states of a given return period. It provides developers with, not only an estimate of the largest significant wave height, but also extreme sea states at other significant wave heights with energy periods that could compromise the survival of a marine structure or service vessel.

Different from the East Coast and Gulf of Mexico, where Atlantic tropical cyclones and hurricanes form, the US northern west coast is subject to the threat of Pacific Northwest (PNW), windstorms. PNW windstorms are mid-latitude extratropical cyclones, which form in the Pacific Ocean and typically occur in the winter. As shown in Figure 3.4, a number of large storm events occurred in November 2009 with maximum significant wave heights exceeding 9 m. Detailed analysis of model results for this period were conducted to evaluate the model performance in simulating large waves during an extreme storm event.

To analyze the model performance on predictions of large waves, a cut-off value of significant wave height for large waves is defined based on the cumulative frequency distribution (Figure 4.12). The 99th percentile of observed data gives H_s ~ 6.2 m. Large waves with H_s > 6.2 m mainly occurred during a number of storm events in November 2009. Therefore, only model results for the period of November are analyzed here. During the storm event in early November, which lasted about 2 days, the WWIII (ST2) baseline model over-predicts the significant wave heights (Figure 4.13). However, with swell dissipation modeled (ST4), results are significantly improved, both in the wave height and the timing of the wave peaks. Interestingly, for the three shorter-duration storms events during the period of November 16–23, both WWIII ST2 and ST4 runs under-predicted the peaks of the wave heights although WWIII ST4 improved the timing of the peaks over WWIII ST2. The improvement of the peak timing is driven by ST4 physics doing a better job in the spectral representation of the waves. The peak frequency due to ST4 physics is much better represented than with ST2 physics. Figure 4.12 also shows WWIII ST4 runs improved the cumulative frequency distribution over WWIII ST2, especially for significant wave heights greater than 1.5 m, which is also demonstrated in the time-series comparison in Figure 4.13. Similar improvements are shown for SWAN-NS model predictions, as shown in Figure 4.14.

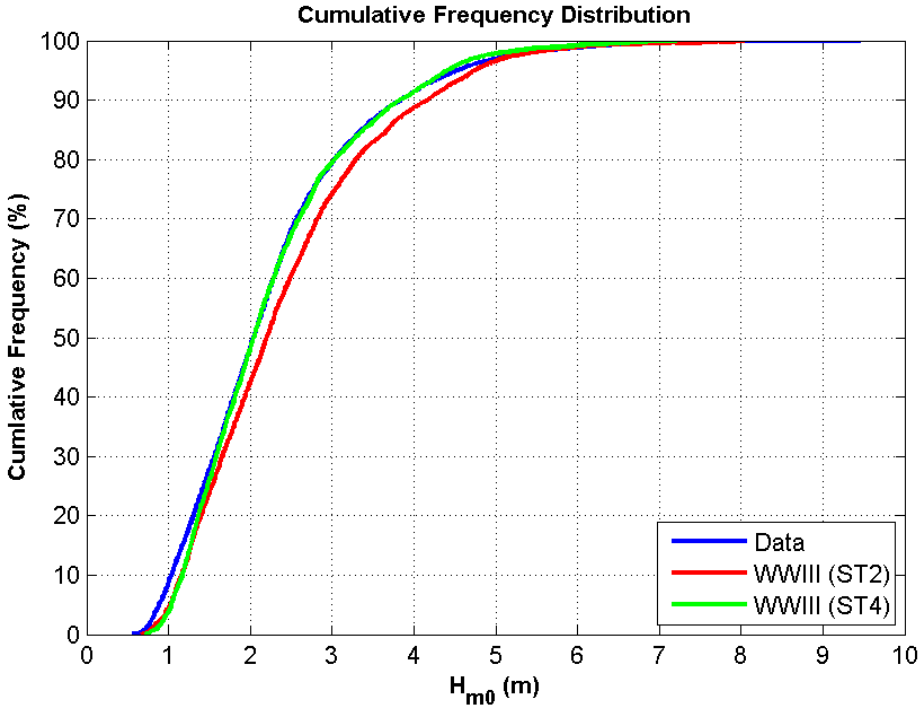

Figure 4.12. Cumulative frequency distributions of significant wave heights derived from WWIII simulations and observations at the NDBC Buoy 46050 site.

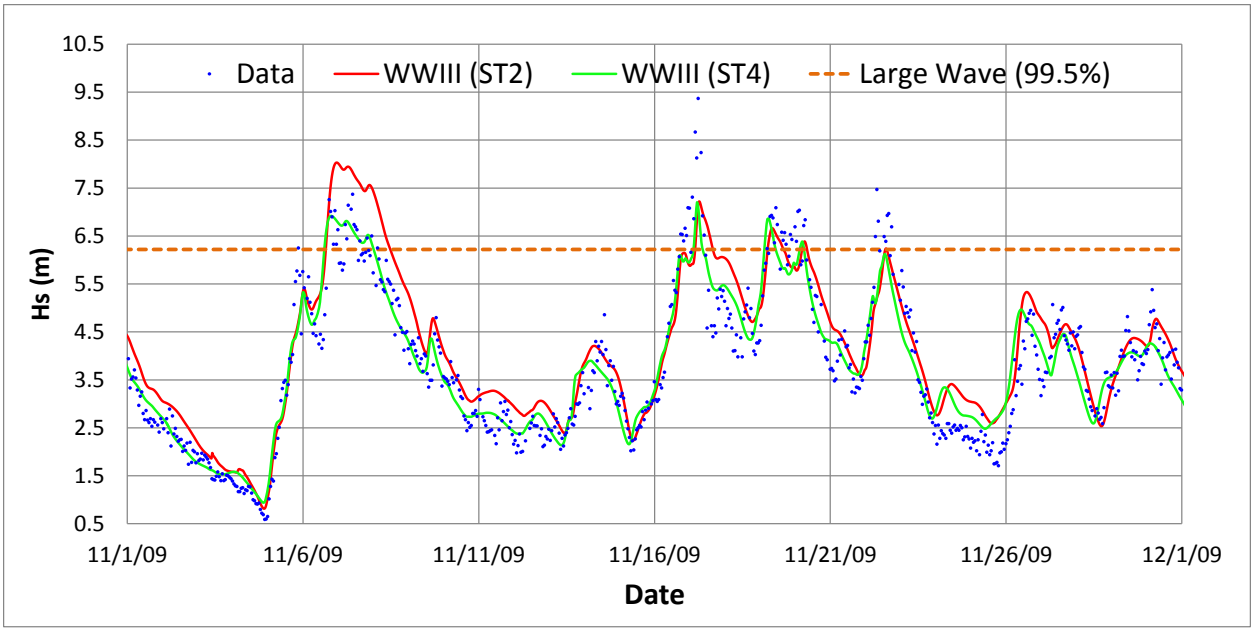

Figure 4.13. Comparisons of significant wave heights for WWIII (ST2 and ST4) and observations in November 2009.

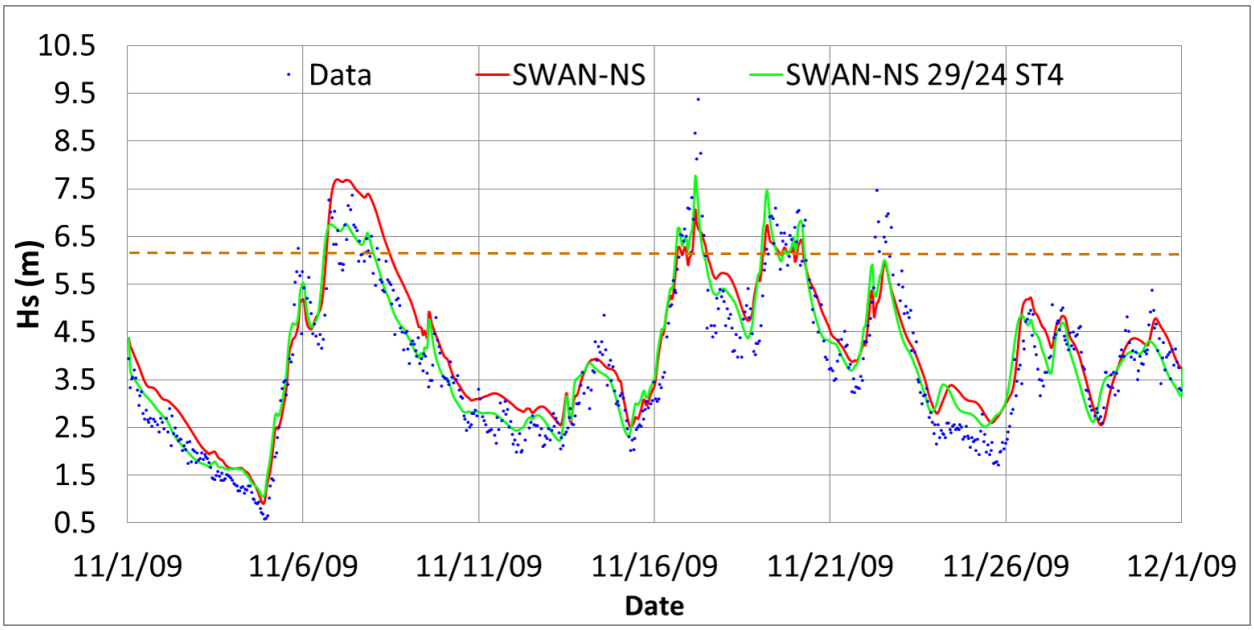

Figure 4.14. Comparisons of significant wave heights for SWAN-NS (ST2 and ST4) and observations in November 2009.

4.5 Computational Requirements

Computational requirements are summarized in Table 4.2 for SWAN-NS, SWAN-S, and WWIII simulation runs. The SWAN simulation requirements assume 16-core CPU platforms, which are widely available at reasonable cost. SWAN simulations in the present study were performed using a 16-core

RHEL 6.4 Linux based operating system (OS) platforms with Intel Xeon E7-4880 processors rated at 2.5 GHz clock speeds, with 37.5 MB L3 Cache, and 1 TB RAM. The WWIII simulations were performed using a 14-node computing cluster with a total of 344 cores. Each CPU is 2 x Opteron 2374 HE (2.2 GHz, Quad Core, SktF, 512 KB/Core L2 Cache, 6 MB L3 Cache) 55 W 45 nm with Mellanox ConnectX QDR (40 GB/s) Single Port Infiniband. The NIC is a Dual Gigabit NIC (Intel 82576).

Table 4.2. SWAN and WWIII computational requirements.

Run ID	Description	Hours (Days) 16 Cores	CPU-hours
SWAN-NS	NS, ST2, 29x24	848 (35.3 days)	13572
SWAN-S	S, ST2, 29x24	46 (1.9 days)	731
SWAN-NS	NS, ST2, 50x36	1689 (70.4 days)	27031
SWAN-S	S, ST2, 50x36	65 (2.7 days)	1036
SWAN-NS	NS, ST4, 29x24	840 (34.9 days)	13435
SWAN-S	S, ST4, 29x24	46 (1.9 days)	739
		256 Cores	
WWIII	ST2, 29x24	123 (5.1 days)	31488
WWIII	ST2, 37x36	219 (9.1 days)	56064
WWIII	ST2, 50x36	295 (12.3 days)	75520
WWIII	ST4, 29x24	140 (5.8 days)	35840

These results indicate a significant increase in CPU-hours when modeling the unsteady term in the action balance equation using the nonstationary mode of SWAN. As expected, a significant increase is observed when increasing the spectral resolution, and virtually no change is observed when accounting for swell dissipation, because it is only implemented through the open wave boundary forcing imposed by the WWIII (ST4) L3 grid model.

5.0 Conclusions

A wave model test bed is established to benchmark, test and evaluate spectral wave models and modeling methodologies (i.e., best practices) for predicting the wave energy resource parameters recommended by the International Electrotechnical Commission, IEC TS 62600-101Ed. 1.0 ©2015. Among other benefits, the model test bed can be used to investigate the suitability of different models, specifically what source terms should be included in spectral wave models under different wave climate conditions and for different classes of resource assessment. The overarching goal is to use these investigations to provide industry guidance for model selection and modeling best practices depending on the wave site conditions and desired class of resource assessment. Modeling best practices are reviewed, and limitations and knowledge gaps in predicting wave energy resource parameters are identified.

Third generation (3G) spectral wave models are evaluated, including WaveWatch III with the ST2 physics package (WWIII ST2), WWIII with the ST4 physics package (WWIII ST4), SWAN with open-wave boundary inputs from WWIII (ST2), and SWAN with open-wave boundary inputs from WWIII (ST4). A nested structured grid approach is employed to provide open-wave boundary conditions to a 60 km x 60 km local model domain. Model performance, aka *model skill*, is defined by evaluating half-a-dozen standard performance metrics based on a comparison of the predictions of six IEC wave resource parameters derived by model hindcasts to those derived from buoy measurements. Potential improvements in model performance, e.g., those due to increased spectral resolution, are quantified by comparing these same metrics with baseline model test cases.

The baseline model test cases are designed to meet or exceed IEC TS 62600-101Ed. 1.0 requirements for *feasibility class* resource assessments. The local model domain grid size is 12" x 10" (~300 m), simulated two-dimensional wave spectra are predicted hourly, and discretized with 29 frequency bins and 24 direction bins, using a logarithmic increment factor of 1.1, and a minimum frequency of 0.035 Hz, which gives the maximum frequency of 0.505 Hz. NOAA/NCEP CFSR data, at 0.5-degree (~50 km) spatial resolution and hourly intervals, is used for wind forcing. All models employ source terms for *design class* resource assessments, including terms for linear and exponential wind growth, and dissipation terms that simulate whitecapping, quadruplet wave interaction, wave breaking and bottom friction. Default parameter settings for these source term models are used; i.e., no coefficients in any source terms are calibrated to measurements.

As a model test-bed study, the present study lays the groundwork for the evaluation of 3G phase-averaged wave models, and modeling methodologies for wave resource assessment and characterization. Computational requirements for running these models are also evaluated to balance trade-offs between model performance and computational cost.

The common practice of employing nested structured grids to impose open wave boundary conditions on a local grid is successfully employed to generate high-resolution wave climate hindcasts for the purpose of feasibility (Class 2) or design (Class 3) wave resource assessments as recommended by IEC 62600-101 TS. In the present study, the local model domain, with a grid resolution of 12" x 9" was nested in three WWIII grids of increasing resolution. Although, the present study did not examine the effects of the ratios of nested-grid resolutions, it followed guidelines provided by NOAA (Tolman et al. 2014).

For the baseline model test case, a comparison of the six IEC parameters time series showed good agreement between WWIII simulations and NDBC buoy measurements. Predicted time series for these six parameters from the SWAN model, both in nonstationary and stationary modes, are comparable to

those from the present study's WWIII (ST2) model; and likewise provide confidence in the SWAN model settings; although small differences between WWIII and SWAN simulations are observed.

Differences between the present study's baseline models are expected due to several factors. First, the WWIII (ST2) model's open wave boundary forcing is two-way nested, while the SWAN models are only one-way nested. Second, the WWIII (ST2) model used a third-order accurate scheme compared to second-order accurate schemes employed by the SWAN-NS and SWAN-S models. Third, the models employ different dissipation models.

Investigations are limited to examining spectral resolution (both frequency and direction), swell dissipation, and nonstationary effects for the SWAN model. Increasing the spectral resolution, specifically almost doubling the number of frequency bins, and increasing the direction bins by 50 percent, is found to provide no improvement in WWIII or SWAN model skills (in terms of predicting wave resource parameters). However, further analysis may be necessary to evaluate the effect of the spectral resolution of the wave energy spectral distribution. Model insensitivity to spectral resolution was likely due to the large depth (128 m) and the absence of any bathymetric or geometric features at the point of comparison. Model predictions may still be sensitive to spectral resolution in the shallow-water areas or regions with the complex geometry of coastlines and therefore additional sensitivity simulations and analysis will be necessary in future studies.

Better representations of growth and dissipation, including swell dissipation, either directly in WWIII using the ST4 package, or indirectly in SWAN by inputting WWIII (ST4) open wave boundary conditions, generally improve model performance, but with mixed results. It improves predictions of significant wave height compared to the baseline model that does not include these physics, but predictions of energy period are not as good. The results support claims that accounting for swell dissipation reduces the overestimation of significant wave height by Ardhuin et al. (2009). Notably, for the purpose of wave resource assessment and characterization, it improves predictions of omnidirectional wave power density.

The SWAN model's sensitivity to the unsteady term in the spectral wave action balance equation is examined by comparing the performance of SWAN in stationary (SWAN-S) and nonstationary (SWAN-NS) modes. The model performance of SWAN in nonstationary mode is better than it is in stationary mode, but differences in performance are marginal, and the computational requirements, measured in CPU-hours, are an order of magnitude less when running in stationary mode. This supports recommendations by The SWAN Team (2015) to use the stationary mode when model domain dimensions are less than 100 km. However, SWAN-S still requires open wave boundary conditions from WWIII. Regional WWIII models with a grid resolution similar to the L3 model in the present study would be valuable for establishing these boundary conditions for WEC developers, consultants, and state and federal agencies interested in performing their own Class 2 (feasibility) and Class 3 (design) resource assessments.

For the purpose of evaluating model performance, model predicted parameters were compared with those derived from buoy data at a depth of 128 m. Therefore, the present study did not evaluate the performance of these models at shallow depths where complex nearshore processes occur. Although the majority of WEC technologies are expected to be designed for nearshore deployments at depths between 50 and 200 m, future investigations should evaluate the accuracy of wave model predictions at shallow depths at less than 30 m. The availability of shallow directional wave measurements within the model test bed will enable such investigations, but the periods of record for these measurements are limited to only a couple of months. Therefore, long-term AWAC deployments at shallow depths are recommended.

Participation by other researchers in future modeling studies at this model test bed is encouraged, and is facilitated by providing open-source information and data from the DOE's MHK data repository (https://mhkdr.openei.org/). At this repository, one can find links to model input data sets, e.g., the model bathymetry file, open wave boundary data files, and model output files from the present study.

6.0 Recommendations for Future Work

Future investigations should include the benefits of unstructured-grids (over a large model domain of interest), a sensitivity study of model parameter settings, a comparison of the predicted and measured wave spectra for evaluating model performance, evaluation of model performance in shallow nearshore environments, large wave predictions, and a longer simulation period.

Inaccurate wind forcing seems to be one of the most important factors affecting the performance of model prediction of wave climates, especially in the nearshore regions. It is a valid next step to evaluate different wind products as well as assimilate observed wind data into the model wind forcing. Although sensitivity analysis with high-frequency resolution did not show noticeable improvements in wave resource parameters, it is necessary to investigate what the lower limit of frequency resolution is and its effect on wave spectral distribution.

The availability of AWAC data in 2005 (July–September) is valuable for evaluating the model's ability to predict wave dynamics in very shallow environments. The use of default settings in the present studies' models establishes a baseline condition for future investigations to improve modeling of large waves, and shows improvements in predicting large waves when modeling growth and swell dissipation effects with the ST4 physics package in WWIII.

7.0 References

Ardhuin F, Chapron B, and Collard F. 2009. Observation of swell dissipation across oceans. *Geophysical Research Letters* (36), L06607.

Ardhuin F, Rogers E, Babanin A, Filipot J-F, Magne R, Roland A, van der Westhuysen A, Queffeulou P, Lefevre J-M, Aouf L, and Collard F. 2010. Semiempirical dissipation source functions for wind-wave models: part I, definition, calibration and validation. *Journal of Physical Oceanography* 40(9):1917–1941.

Ardhuin F, Hanafin J, Quilfen Y, Chapron B, Queffeulou P, and Obrebski M. 2011. Calibration of the "IOWAGA" Global Wave Hindcast (1991-2011) Using ECMWF and CFSR Winds. *Proceedings of the 12th International Workshop on Wave Hindcasting and Forecasting*, Kohala Coast, Hawaii.

Ardhuin F and A Roland. 2013. The development of spectral wave models: coastal and coupled aspects. In the Proceedings of 7th international Conference on Coastal Dynamics, June 24–28, 2013. Arcachon, France.

Battjes, J. A. and J. P. F. M. Janssen, 1978: Energy loss and set-up due to breaking of random waves. in *Proc. 16th Int. Conf. Coastal Eng.*, pp.569–587. ASCE. Cavaleri, L. 2009. Wave modeling – Missing Peaks. *Journal of Physical Oceanography* (39):2757–2778.

Cavaleri, L. and P. Malanotte-Rizzoli, 1981: Wind wave prediction in shallow water: Theory and applications. J. Geophys. Res., 86, No. C11, 10,961-10,973 Chen C, Liu H, and Beardsley RC. 2003. An unstructured, finite-volume, three-dimensional, primitive equation ocean model: application to coastal ocean and estuaries. *Journal of Atmospheric Oceanic Technology* 20:159–186.

Dallman AR and Neary VS. 2014a. Characterization of U.S. Wave Energy Converter (WEC) Test Sites: A Catalogue of Met-Ocean Data. SAND2014-18206, Sandia National Laboratories, Albuquerque, New Mexico.

Dallman, A.R., Neary, V.S., Stephenson, M. 2014b. Investigation of Spatial Variation of Sea States Offshore of Humboldt Bay, CA Using a Hindcast Model. SAND2014-18207, Sandia National Laboratories, Albuquerque, New Mexico.

Drew B, Plummer AR, and Sahinkaya MN. 2009. A review of wave energy converter technology, *Proceedings of the IMechE, 223 Part A: Journal Power and Wave Energy* 223:887–902.

EPRI (Electric Power Research Institute). 2011. *Mapping and Assessment of the United States Ocean Wave Energy Resource*. EPRI 2011 Technical Report to U.S. Department of Energy, Palo Alto, California.

Hanson, J. L., B. A. Tracy, H. L. Tolman and D. Scott, 2006: Pacific hindcast performance evaluation of three numerical wave models. in *9* th *international workshop on wave hindcasting and forecasting, JCOMM Tech. Rep.34*. Paper A2.

Hasselmann, S., K. Hasselmann, J. H. Allender and T. P. Barnett, 1985: Computations and parameterizations of the nonlinear energy transfer in a gravity-wave spectrum, Part II: parameterizations of the nonlinear energy transfer for application in wave models. *J. Phys. Oceanogr.*, 15, 1,378–1,391.
Gagnaire-Renou E, Benoit M, and Forget PH. 2010. Ocean wave spectrum properties as derived from quasi-exact computations of nonlinear wave-wave interactions. J*ournal of Geophysical Research C (Oceans)* 115, C12, C12058, doi:10.1029/2009JC005665.

García-Medina G, Özkan-Haller HT, Ruggiero P, and Oskamp J. 2013. An Inner-Shelf Wave Forecasting System for the U.S. Pacific Northwest. *Weather and Forecasting* 28:681–703.

García-Medina G, Özkan-Haller HT, and Ruggiero P. 2014. Wave resource assessment in Oregon and southwest Washington, USA. *Renewable Energy* 64:203–214.

IAHR (International Association of Hydraulic Research). 1989. List of sea-state parameters. Journal of Waterways, Ports and Ocean Engineering 115:793–808.

IEC (International Electrotechnical Commission). 2015. Marine energy – Wave, tidal and other water current converters – Part 101: Wave energy resource assessment and characterization. IEC TS 62600-101. Edition 1.0.2015-06, Geneva, Switzerland.

Kirincich AR, Lentz SJ, and Barth JA. 2009. Wave-driven inner-shelf motions on the Oregon coast. *Journal of Physical Oceanography* 39:2942–2956.

Janssen, P.A.E.M., 1989: Wave induced stress and the drag of air flow over sea waves, J. Phys. *Oceanogr*., 19, 745-754

Janssen, P. A. E. M., 1991: Quasi-linear theory of of wind wave generation applied to wave forecasting. *J. Phys. Oceanogr.*, 21, 1,631–1,642.

Hasselmann, K., T.P. Barnett, E. Bouws, H. Carlson, D.E. Cartwright, K. Enke, J.A. Ewing, H. Gienapp, D.E. Hasselmann, P. Kruseman, A. Meerburg, P. M¨uller, D.J. Olbers, K. Richter, W. Sell and H. Walden, 1973: Measurements of wind−wave growth and swell decay during the Joint North Sea Wave Project (JONSWAP), Dtsch. Hydrogr. Z. Suppl., 12, A8
Komen, G.J., S. Hasselmann, and K. Hasselmann, 1984: On the existence of a fully developed wind-sea spectrum, J. Phys. *Oceanogr*., 14, 1271-1285

Lenee-Bluhm P, Paasch R, and Özkan-Haller HT. 2011. Characterizing the wave energy resource of the US Pacific Northwest. *Renewable Energy* 36:2106–2119.

Neary V. S., Previsic M., Jepsen R. A., Lawson M. J., Yu Y.-H., Copping A. E., Fontaine A. A., Hallett K. C., Murray D. K., 2014. *Methodology for Design and Economic Analysis of Marine Energy Conversion (MEC) Technologies*. SAND2014-9040, Sandia National Laboratories, Albuquerque, New Mexico.

Qi J, Chen C, Beardsley RC, Perrie W, and Cowles G. 2009. An unstructured-grid finite-volume surface wave model (FVCOM-SWAVE): implementation, validations and applications. *Ocean Modelling* 28:153–166, doi:10.1016/j.ocemod.2009.01.007.

Robertson B, Hiles CE, and Buckham BJ. 2014. Characterizing the near shore wave energy resource on the west coast of Vancouver Island, Canada. *Renewable Energy* 665–678.

Rogers WE and Campbell TJ. 2009. Implementation of curvilinear coordinate system in the WAVEWATCH III model. NRL/MR/7320–09-9193, Naval Research Laboratory Stennis.

Saha S, Moorthi S, Pan H, Wu X, Wang J, and Coauthors. 2010. The NCEP Climate Forecast System Reanalysis. *Bulletin of the American Meteorological Society* 91:1015–1057, doi:10.1175/2010BAMS3001.1

Sørensen OR, Kofoed Hansen H, Rugbjerg M, and Sørensen LS. 2004. A Third Generation Spectral Wave Model Using an Unstructured Finite Volume Technique. In *Proceedings of the 29th International Conference of Coastal Engineering*, 19–24 September 2004, Lisbon, Portugal.

Sun Y, Chen C, Beardsley RC, Xu Q, Qi J, and Lin H. 2013. Impact of current-wave interaction on storm surge simulation: A case study for Hurricane Bob. *Journal of Geophysical Research (Oceans)* 118:2685–2701

The SWAN Team. 2015. SWAN: User Manual. Delft University of Technology, Environmental Fluid Mechanics Section, available from *http://www.swan.tudelft.nl (*SWAN Cycle III version 41.01A, 2015).

Tolman HL and Chalikov D. 1996. Source terms in a third-generation wind wave model. *Journal of Physical Oceanography* 26:2497–2518.

Tolman HL. 2010. WAVEWATCH III® development best practices. Tech. Note 286, Ver. 0.1, NOAA/NWS/NCEP/MMAB, 19 pp.

Tolman H. and the WAVEWATCH III® Development Group. 2014. User manual and system documentation of WAVEWATCH III® version 4.18. Available from *http://polar.ncep.noaa.gov/waves/wavewatch/* (Version 4.18, 2014).

Tucker MJ and Pitt EG. 2001. Waves in Ocean Engineering. Elsevier Ocean Engineering Book Series, Vol. 5, Elsevier Science Ltd., First Ed.

van Nieuwkoop JCC, Smith HCM, Smith GH, and Johanning L. 2013. Wave resource assessment along the Cornish coast (UK) from a 23-year hindcast dataset validated against buoy measurements. *Renewable Energy* 58:1–14.

Vimont DJ. 2004. The Contribution of the Interannual ENSO Cycle to the Spatial Pattern of Decadal ENSO-Like Variability. J*ournal of Climate* 18:2080–2092.

Wang XL, Swail VR (2001) Changes of Extreme Wave Heights in Northern Hemisphere Oceans and Related Atmospheric Circulation Regimes. *Journal of Climate* 14:2204-2221.

WAMDI Group. 1988. The WAM model – a third generation ocean wave prediction model. *Journal of Physical Oceanography* 18:1775–1810.

Zijlema, M., 2010: Computation of wind-wave spectra in coastal waters with SWAN on unstructured grids. *Coastal Eng.*, 57(3), 267 – 277.

Appendix A

Time-Series Plots of Six IEC Parameters

Appendix A

Time-Series Plots of Six IEC Parameters

A.1 WWIII Time-Series Plots

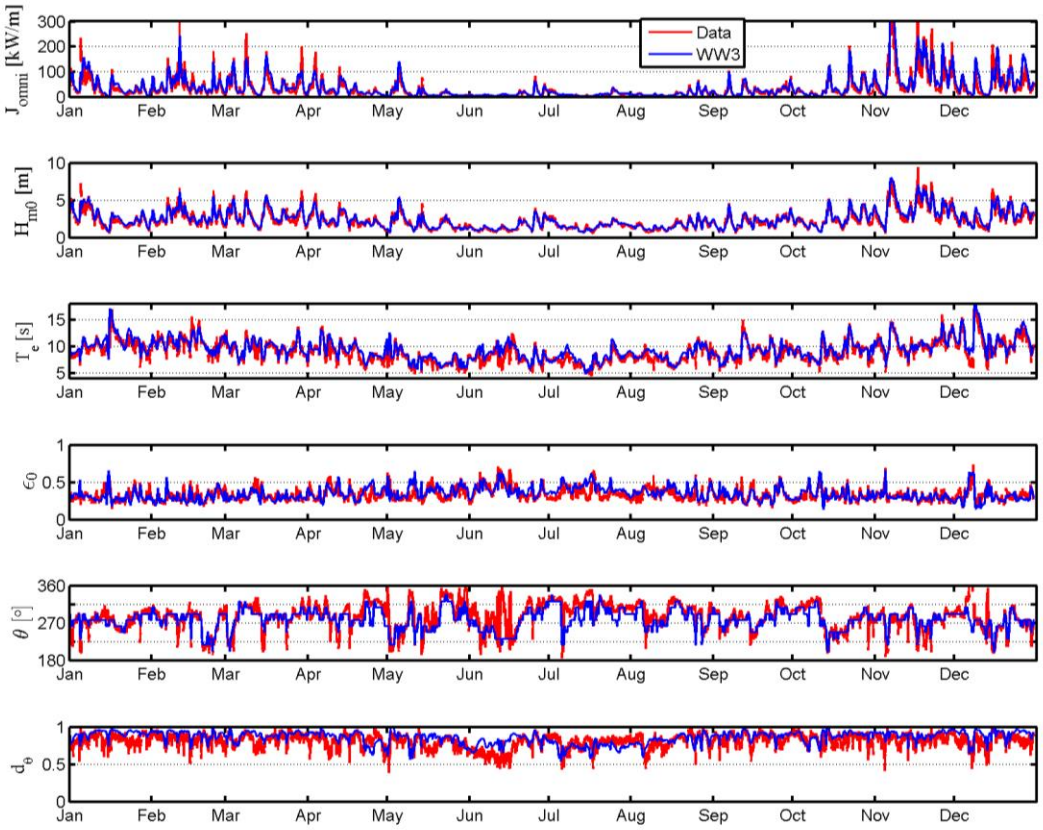

Figure A.1. Comparisons of model-simulated six IEC parameters with observed data at NDBC Buoy 46050 for the baseline condition with 29 frequency bins and 24 direction bins.

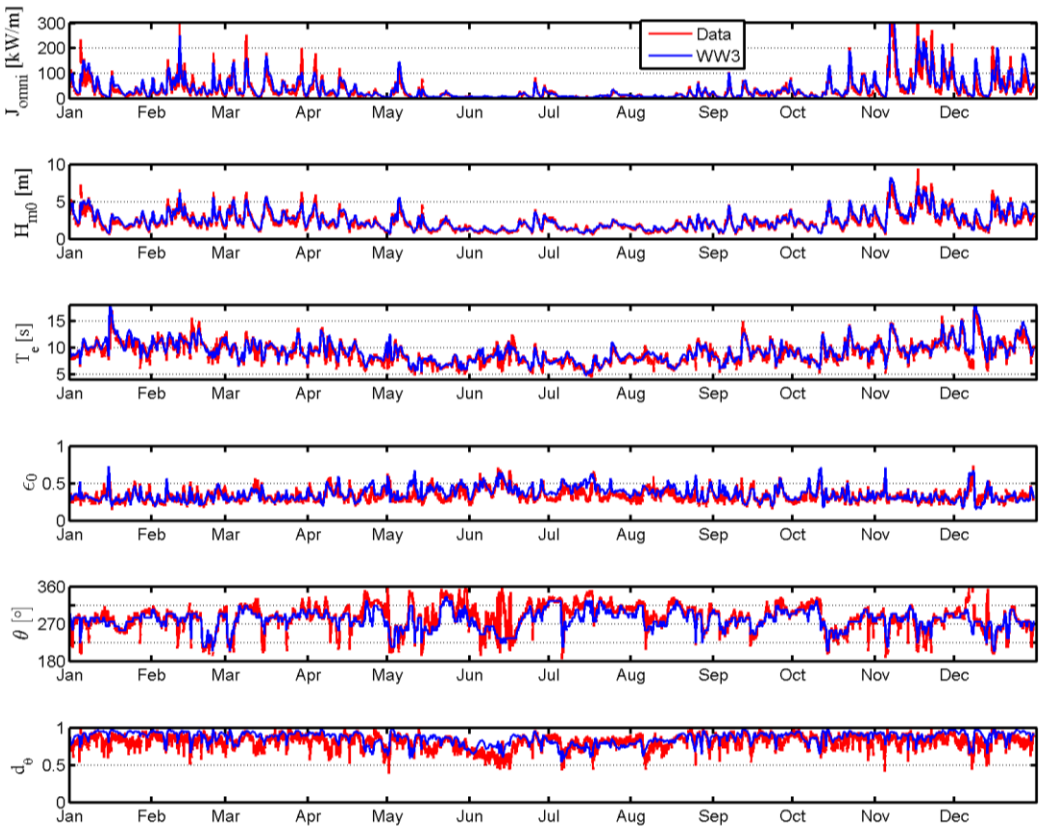

Figure A.2. Comparisons of model-simulated six IEC parameters with observed data at NDBC Buoy 46050 for sensitivity run with 37 frequency bins and 36 direction bins.

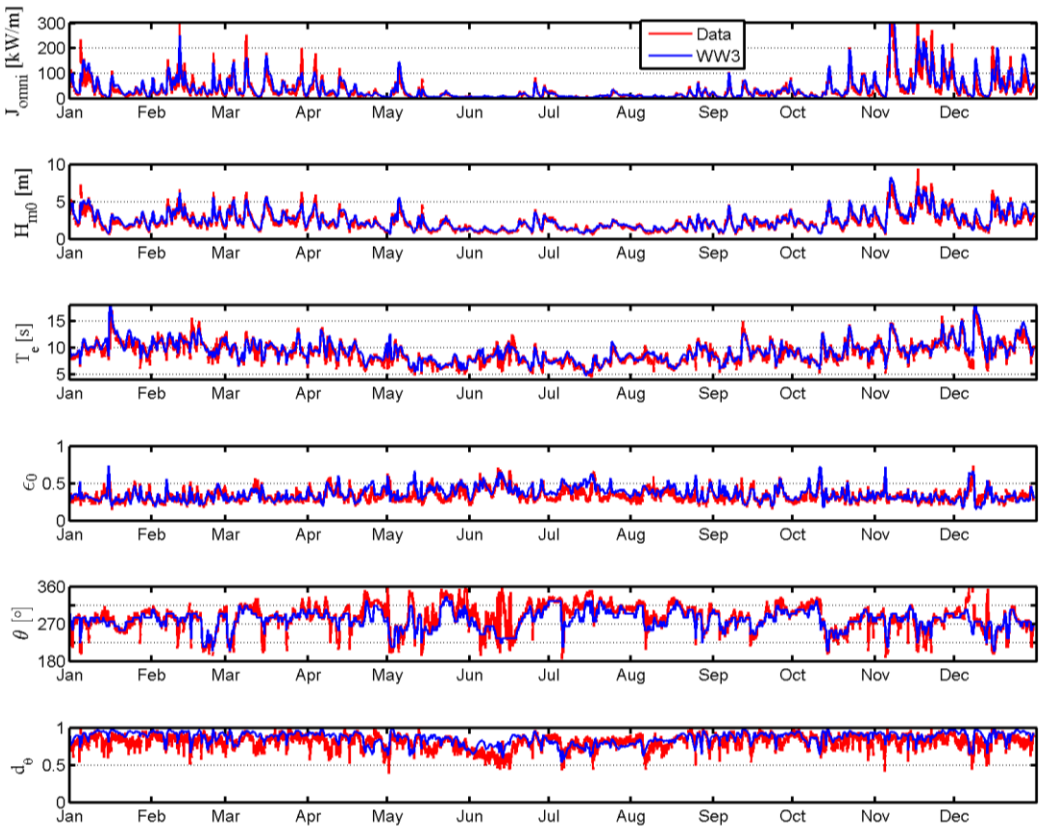

Figure A.3. Comparisons of model-simulated six IEC parameters with observed data at NDBC Buoy 46050 for sensitivity run with 50 frequency bins and 36 direction bins.

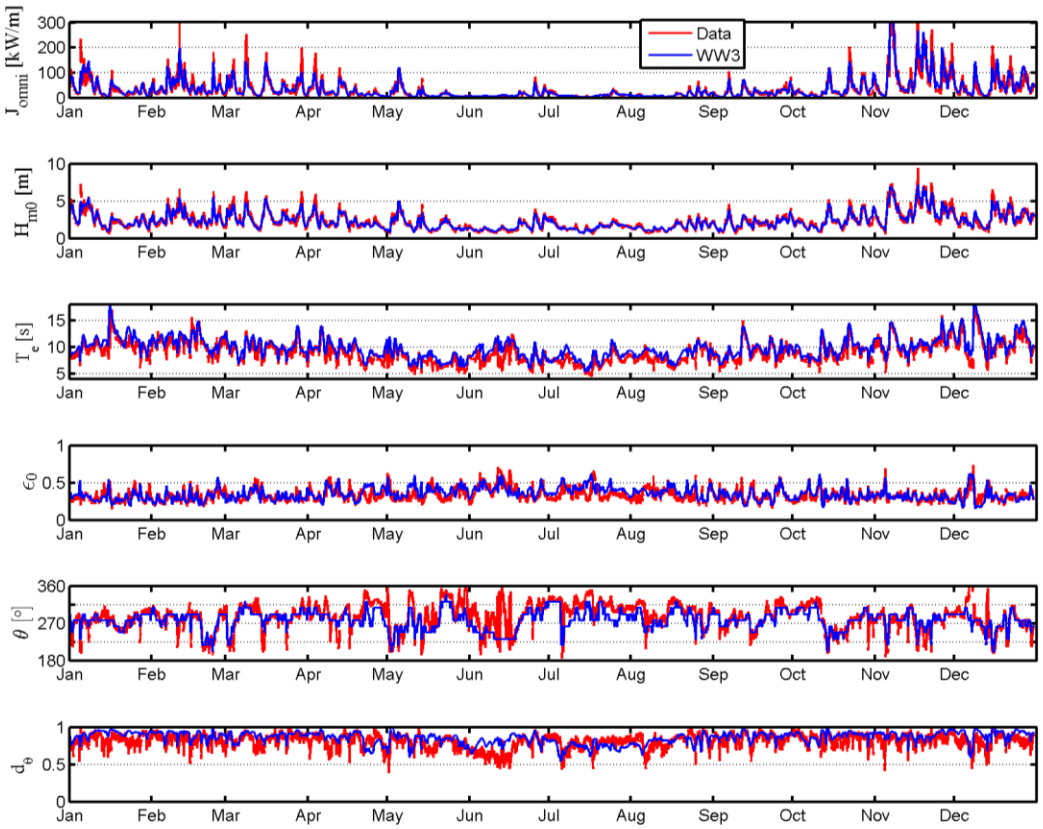

Figure A.4. Comparisons of model-simulated six IEC parameters with observed data at NDBC Buoy 46050 for sensitivity run with 50 frequency bins and 36 direction bins

A.2 SWAN Time-Series Plots

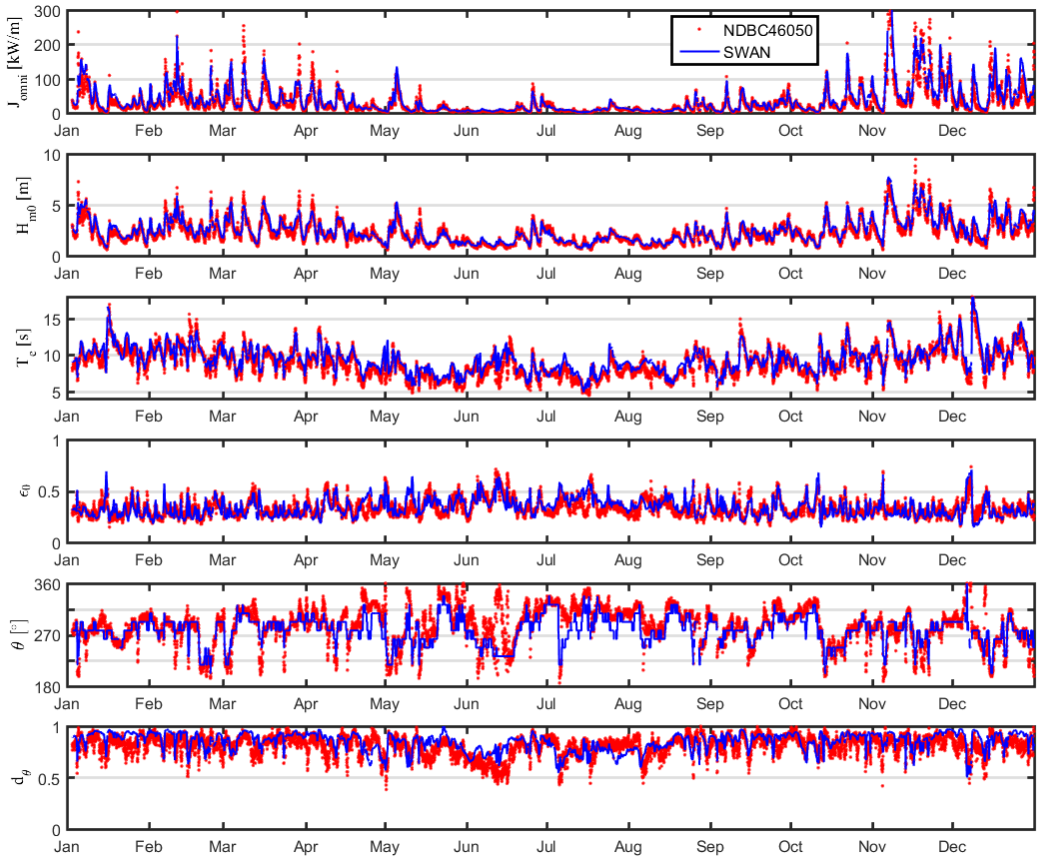

Figure A.5. Comparisons of SWAN-NS baseline model-simulated six IEC parameters with observed data at NDBC Buoy 46050 for the baseline condition with 29 frequency bins and 24 direction bins. Open wave boundary forcing from WWIII with ST2 physics package.

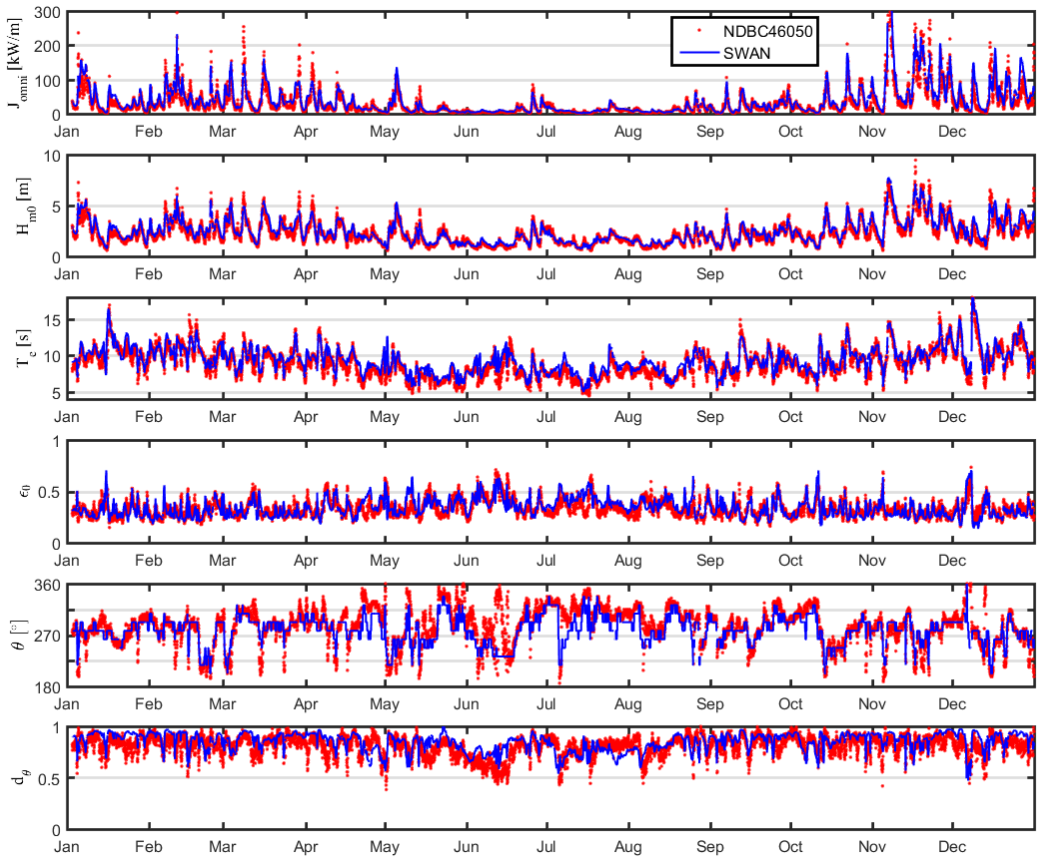

Figure A.6. Comparisons of SWAN-S baseline model-simulated six IEC parameters with observed data at NDBC Buoy 46050 for the baseline condition with 29 frequency bins and 24 direction bins. Open wave boundary forcing from WWIII with ST2 physics package.

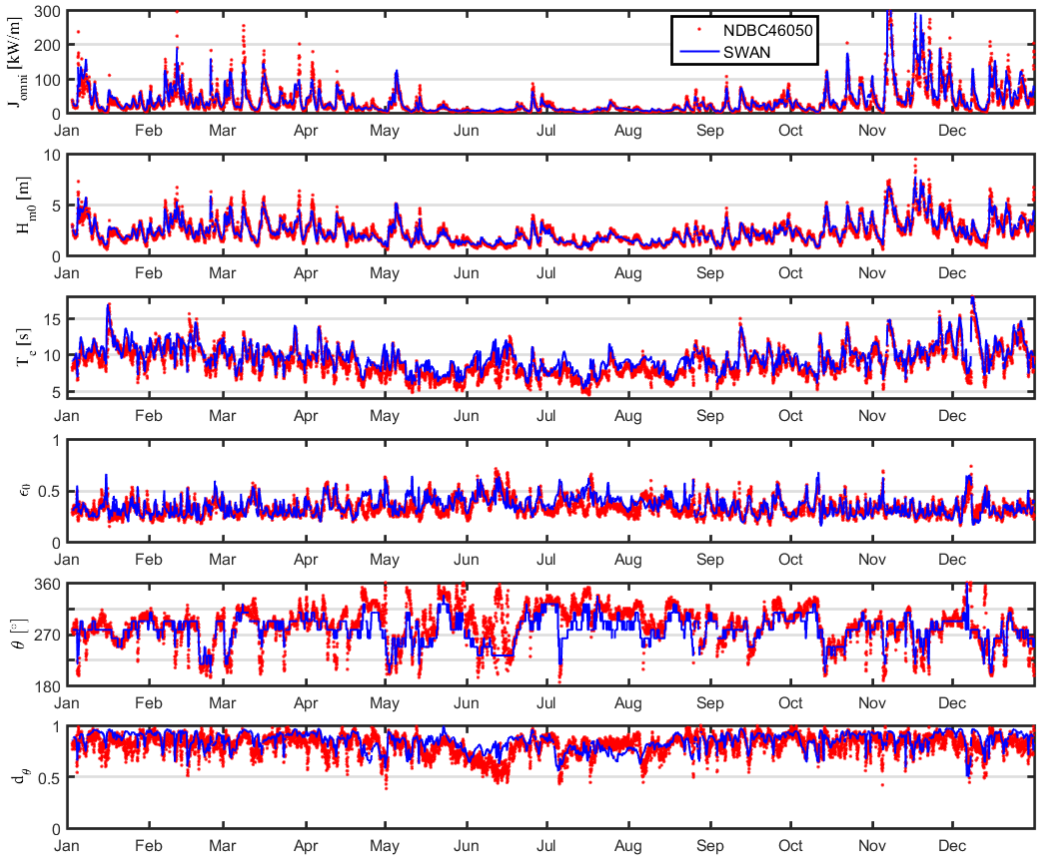

Figure A.7. Comparisons of SWAN-NS model-simulated six IEC parameters with observed data at NDBC Buoy 46050 for the baseline condition with 29 frequency bins and 24 direction bins. Open wave boundary forcing from WWIII with ST4 physics package (swell dissipation).

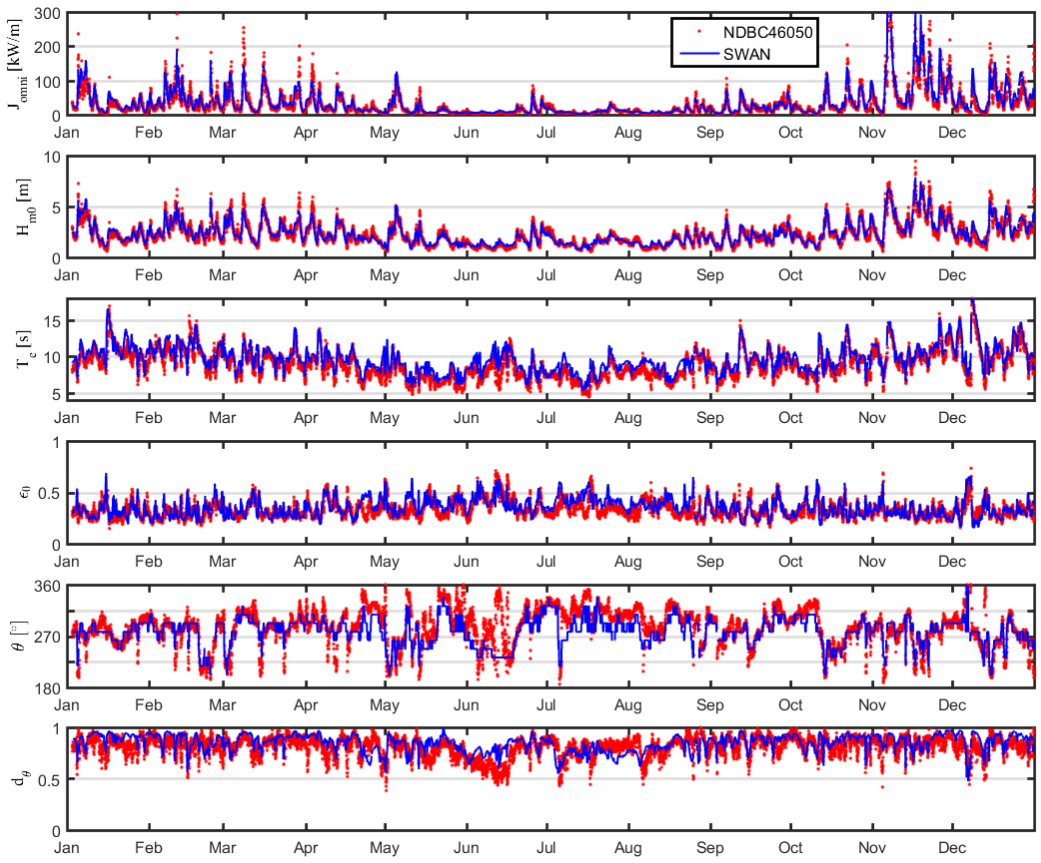

Figure A.8. Comparisons of SWAN-S model-simulated six IEC parameters with observed data at NDBC Buoy 46050 for the baseline condition with 29 frequency bins and 24 direction bins. Open wave boundary forcing from WWIII with ST4 physics package (swell dissipation).

Appendix B

Q-Q Plots

Appendix B

Q-Q PLOTS

B.1 WWIII Q-Q Plots

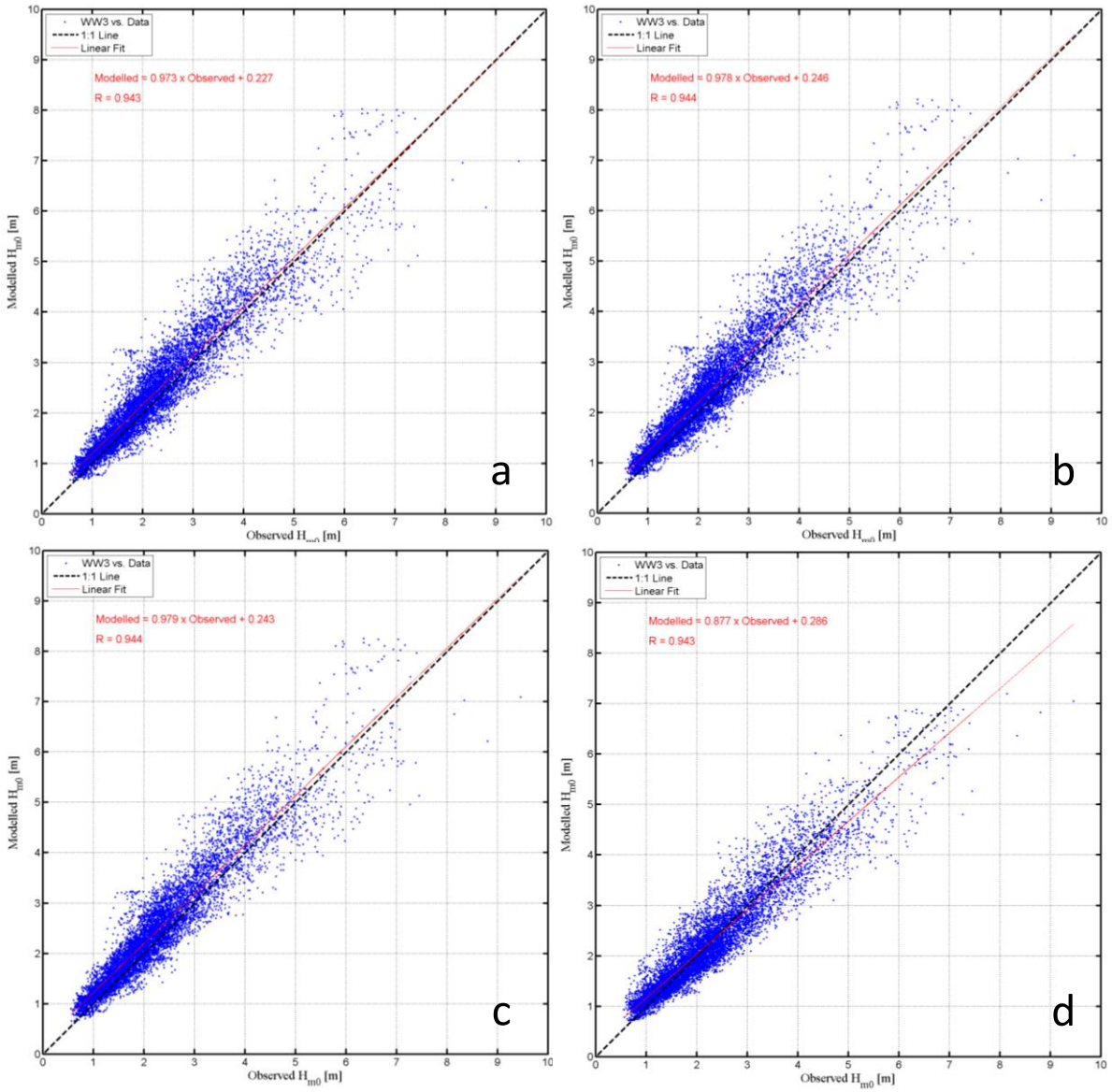

Figure B.1. Scatter plots of significant wave height Hs for WWIII vs data for model runs a) baseline (ST2-29×24), b) sensitivity run (37×36), c) sensitivity (50×36), d) sensitivity (ST4-29×24).

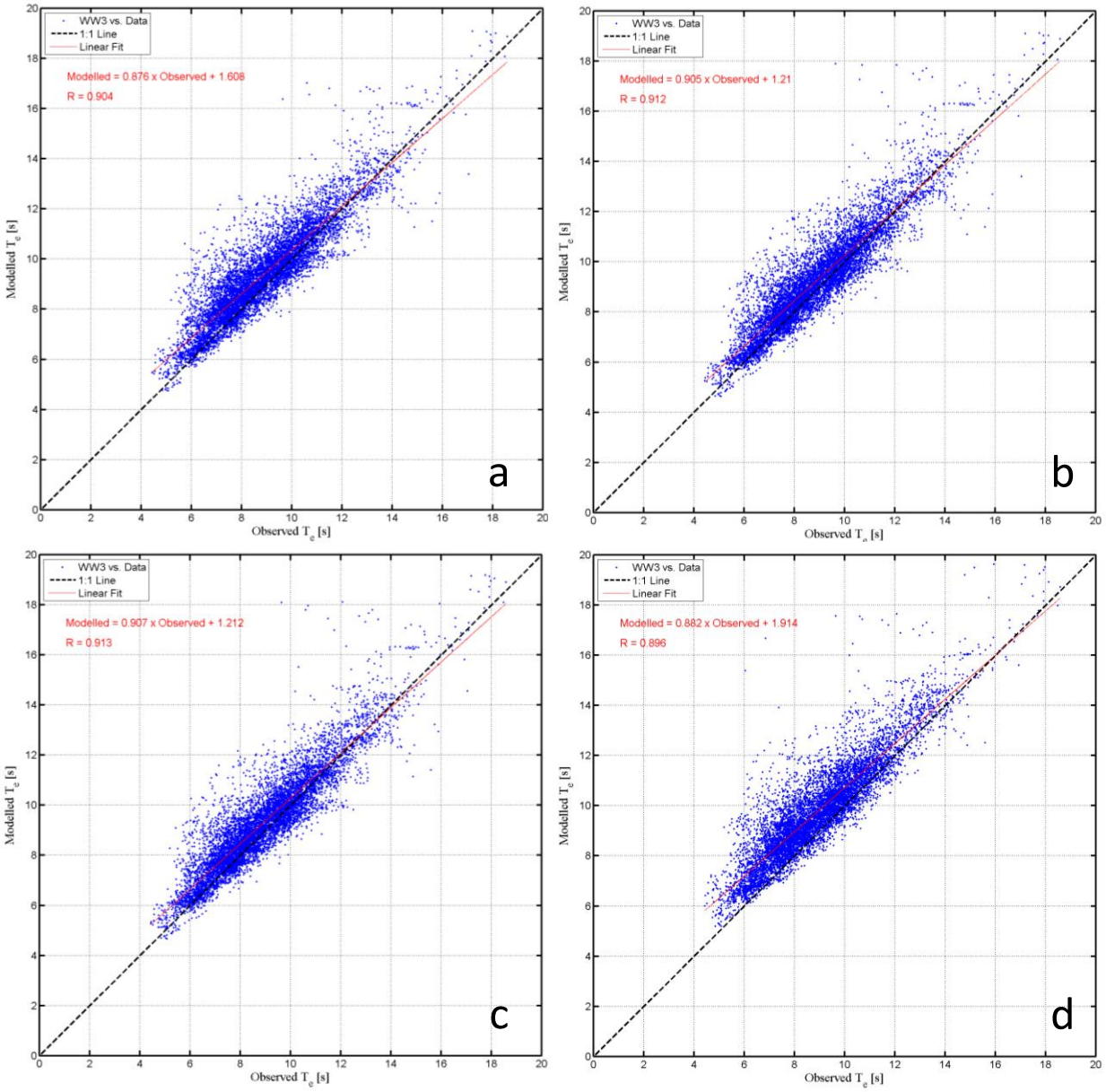

Figure B.2. Scatter plots of energy period Te for WWIII vs data for model runs a) baseline (ST2-29×24), b) sensitivity run (37×36), c) sensitivity (50×36), d) sensitivity (ST4-29×24).

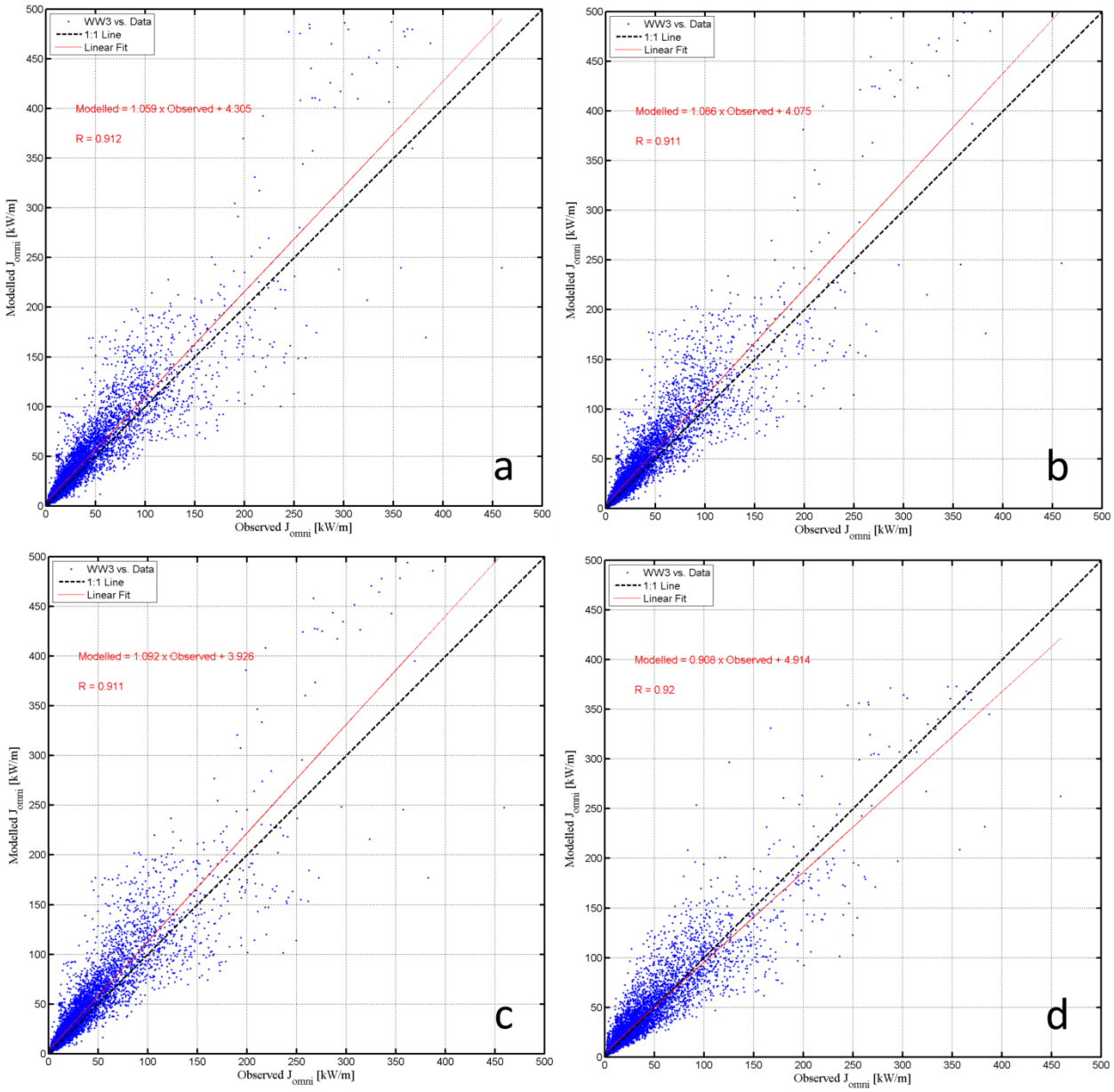

Figure B.3. Scatter plots of omnidirectional wave power *J* for WWIII vs data for model runs a) baseline (ST2-29×24), b) sensitivity run (37×36), c) sensitivity (50×36), d) sensitivity (ST4-29×24).

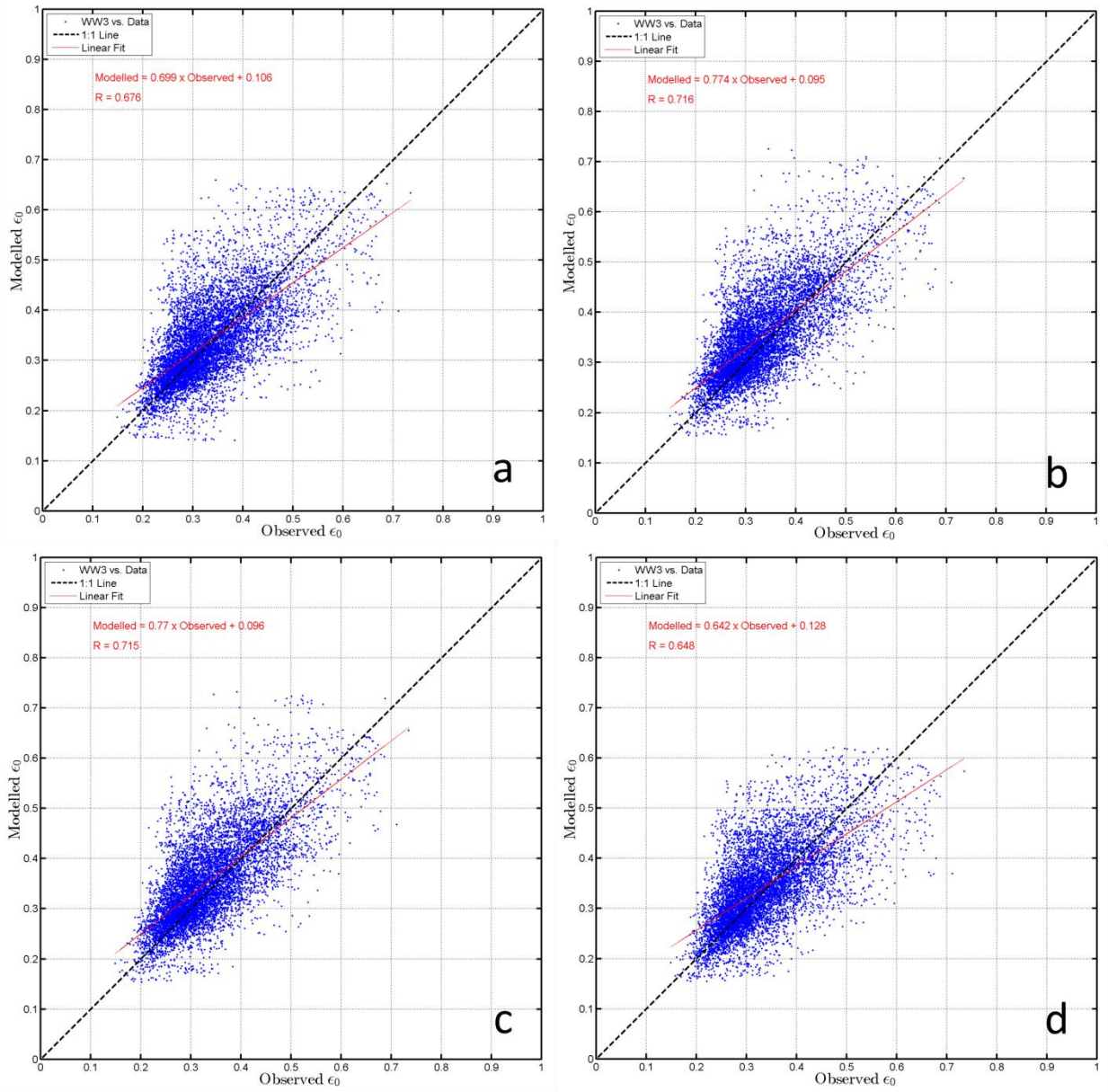

Figure B.4. Scatter plots of spectral width $\boldsymbol{\epsilon_0}$ for WWIII vs data for model runs a) baseline (ST2-29×24), b) sensitivity run (37×36), c) sensitivity (50×36), d) sensitivity (ST4-29×24).

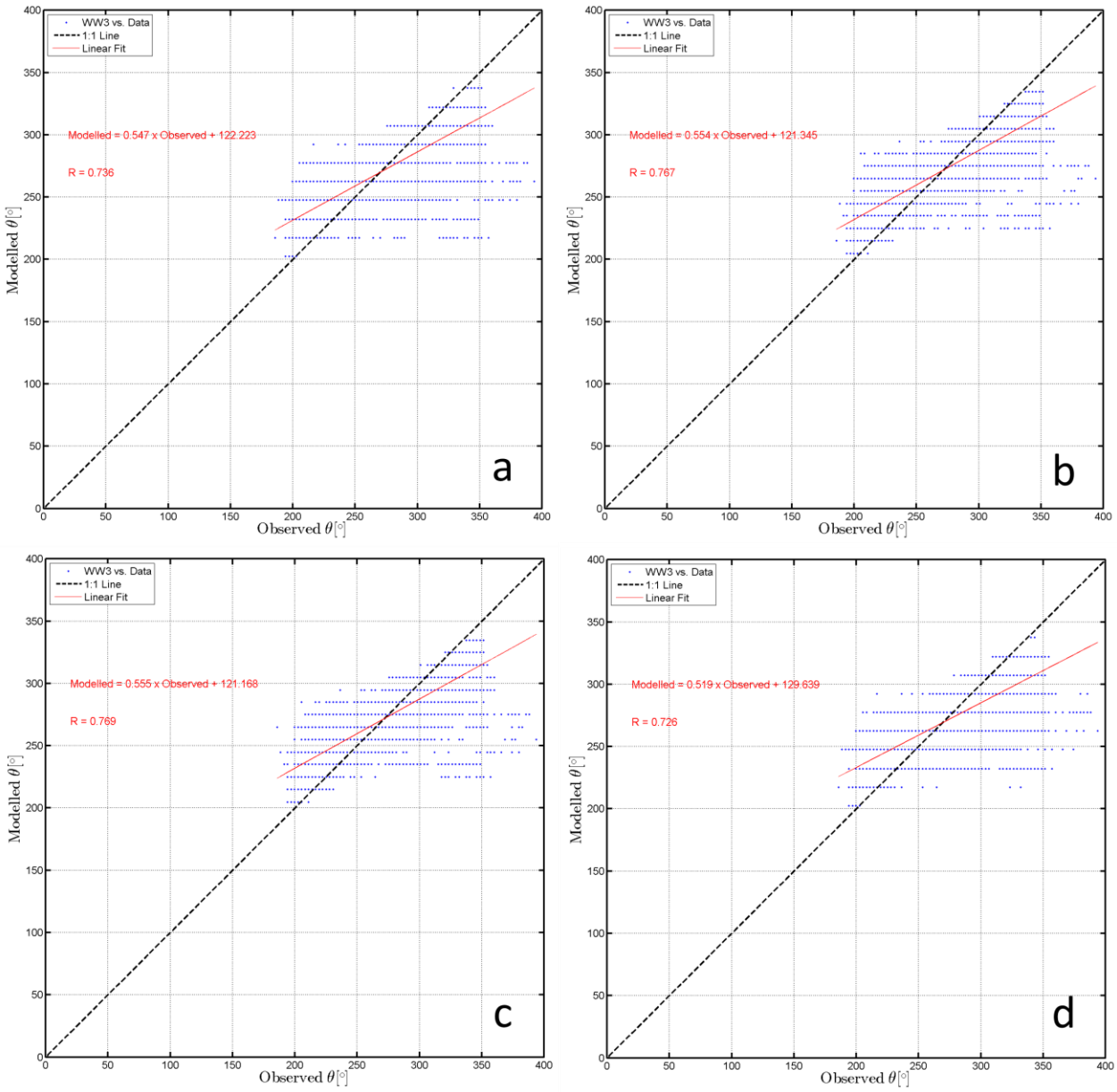

Figure B.5. Scatter plots of direction of maximum directionally resolved wave power $\boldsymbol{d_\theta}$ for WWIII vs data for model runs a) baseline (ST2-29×24), b) sensitivity run (37×36), c) sensitivity (50×36), d) sensitivity (ST4-29×24).

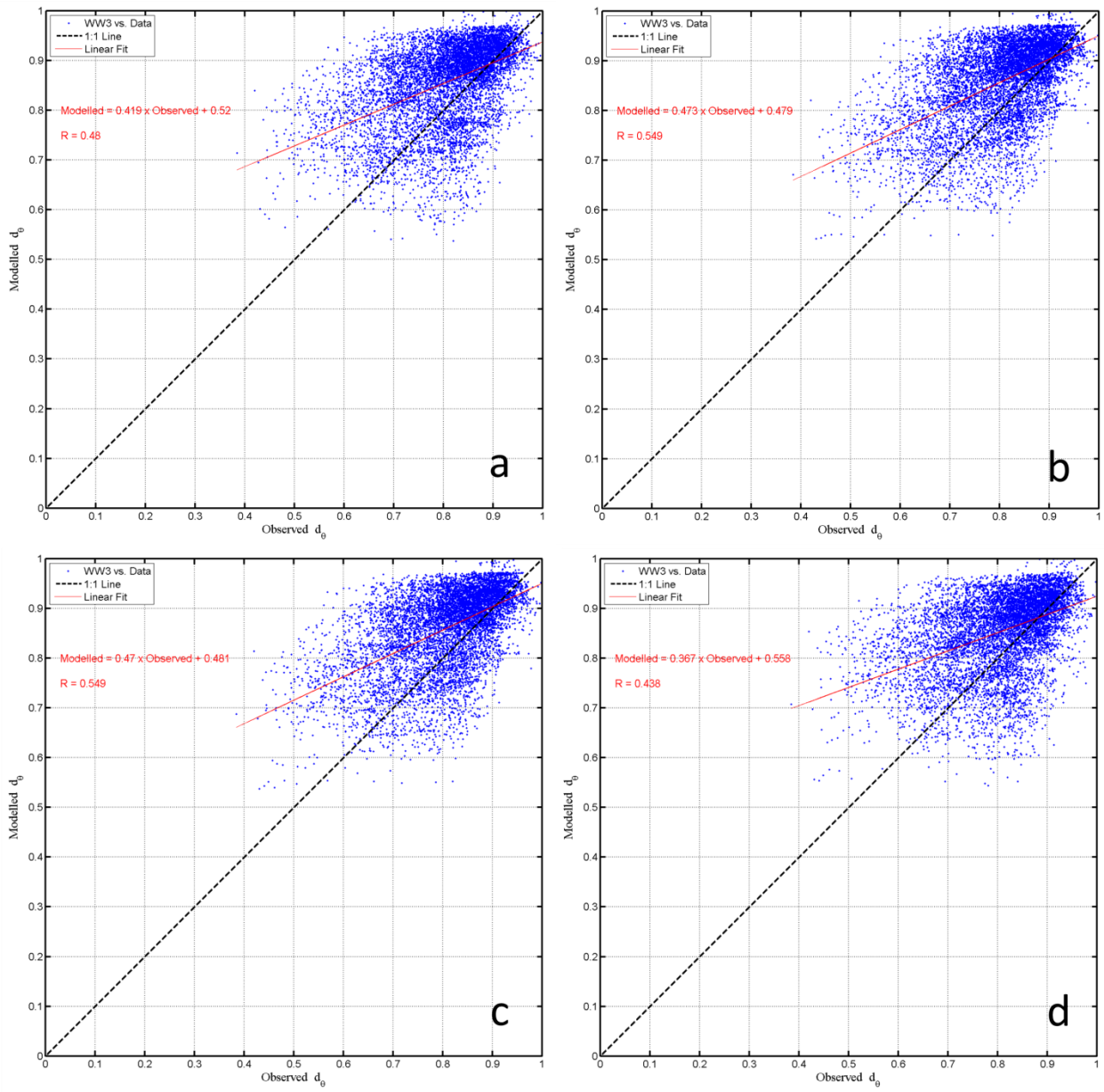

Figure B.6. Scatter plots of directionality coefficient $\boldsymbol{\theta}$ for WWIII vs data for model runs a) baseline (ST2-29×24), b) sensitivity run (37×36), c) sensitivity (50x36), d) sensitivity (ST4-29×24).

B.2 SWAN Q-Q Plots

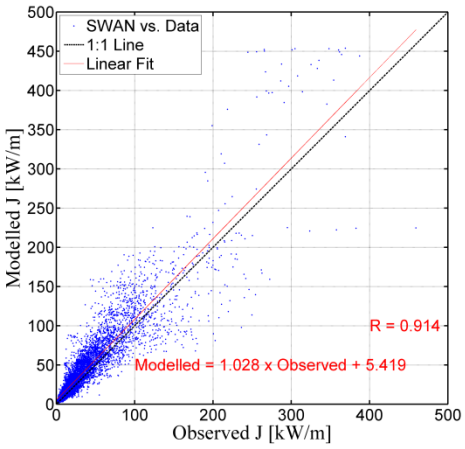

J

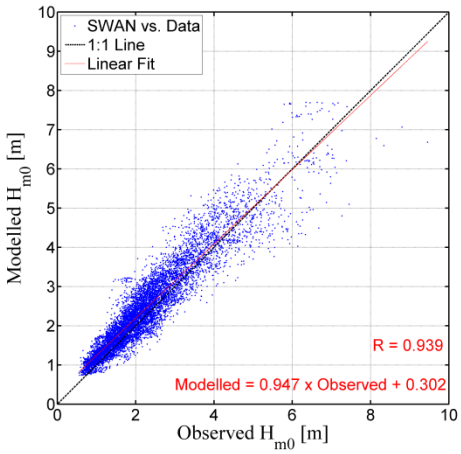

H_{m0}

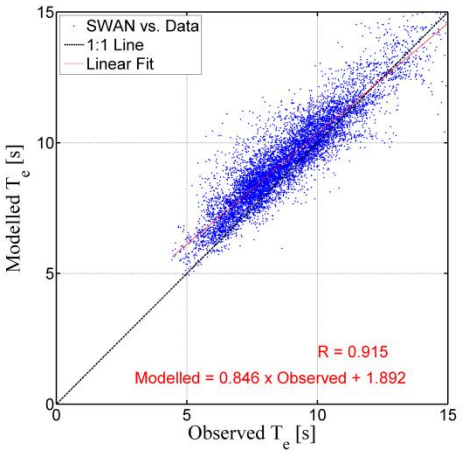

T_e

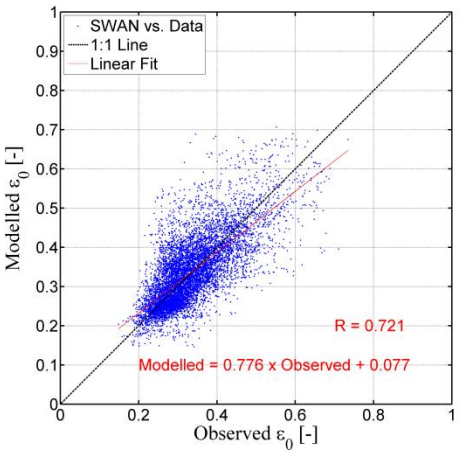

ε_0

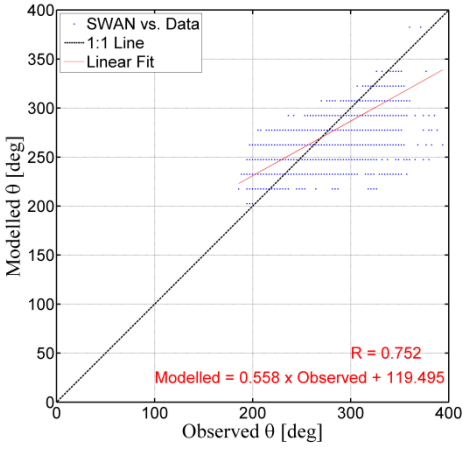

θ

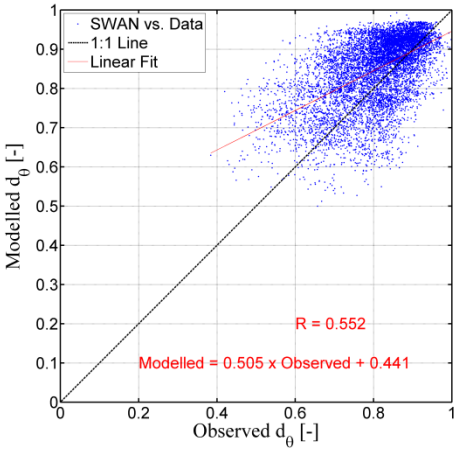

d_θ

Figure B.7. Scatter plots of IEC wave resource parameters for SWAN-NS baseline (ST2-29×24).

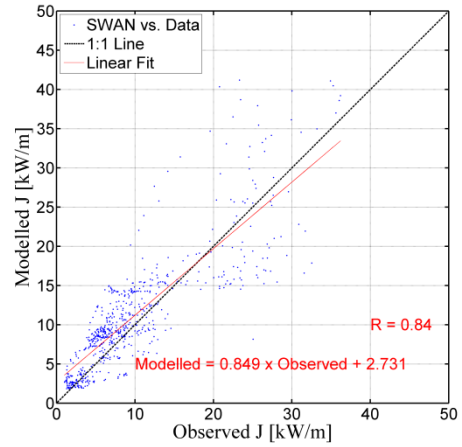

J

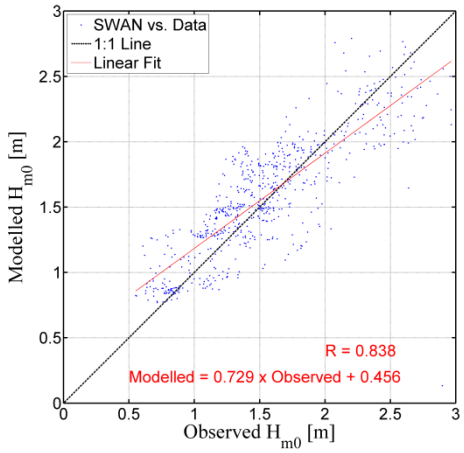

H_{m0}

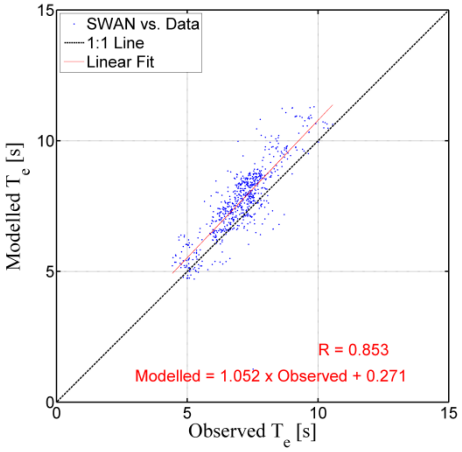

T_e

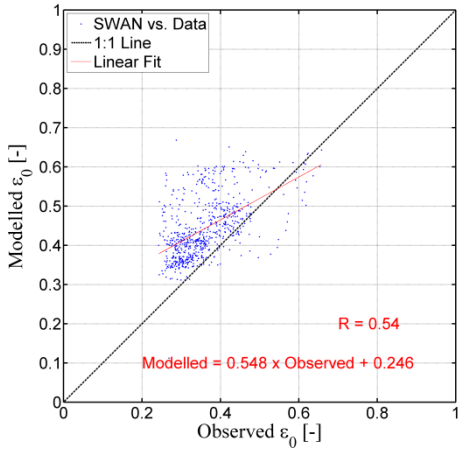

ε_0

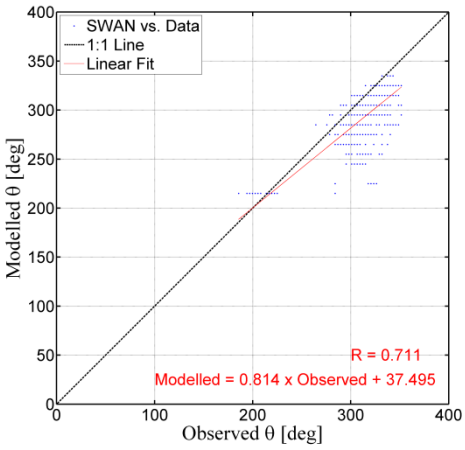

θ

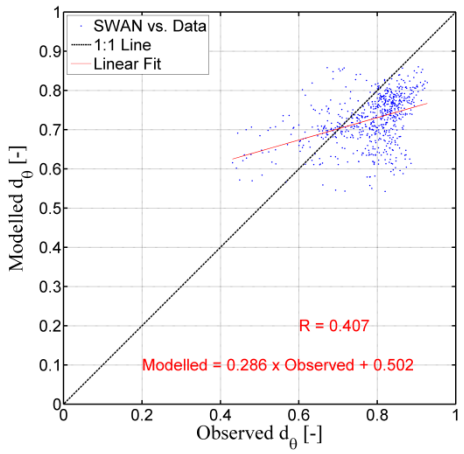

d_θ

Figure B.8. Scatter plots of IEC wave resource parameters for SWAN-NS, July 2009 (ST2-50×36).

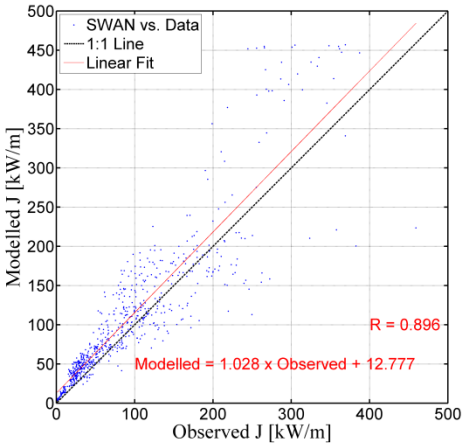

J

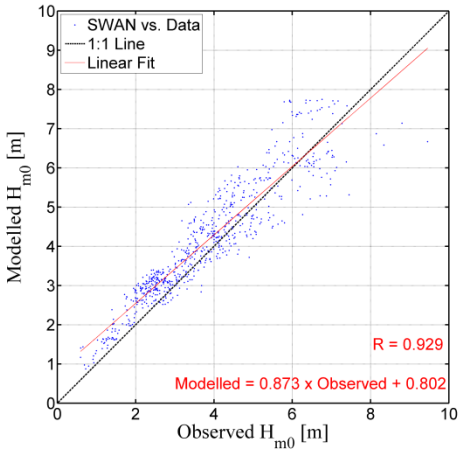

H_{m0}

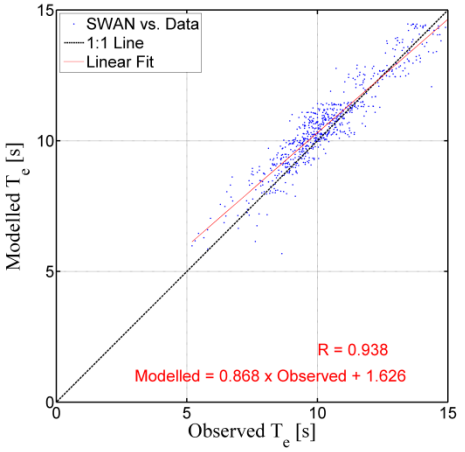

T_e

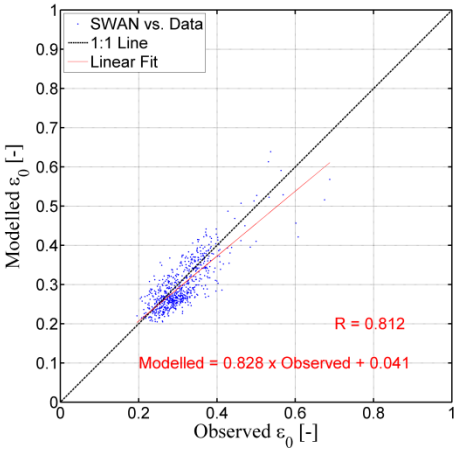

ε_0

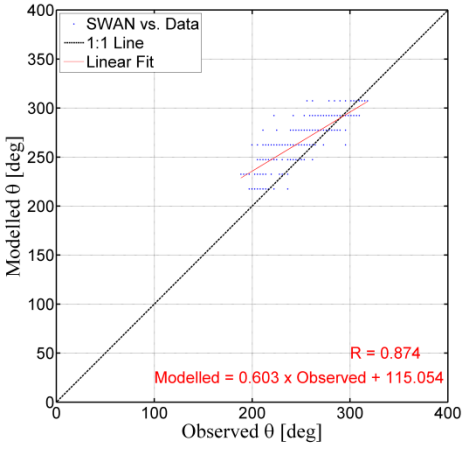

θ

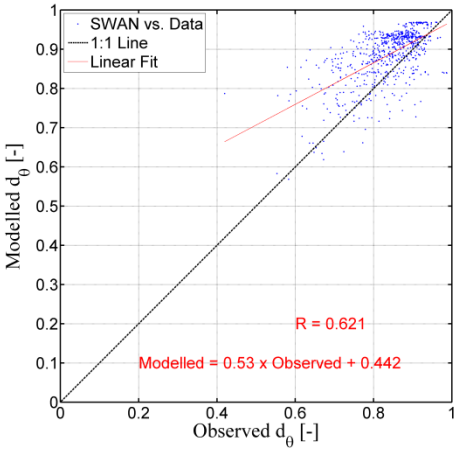

d_θ

Figure B.9. Scatter plots of IEC wave resource parameters for SWAN-NS, November 2009 (ST2-50×36).

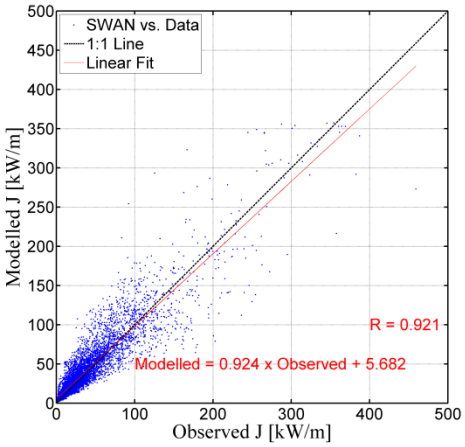

J

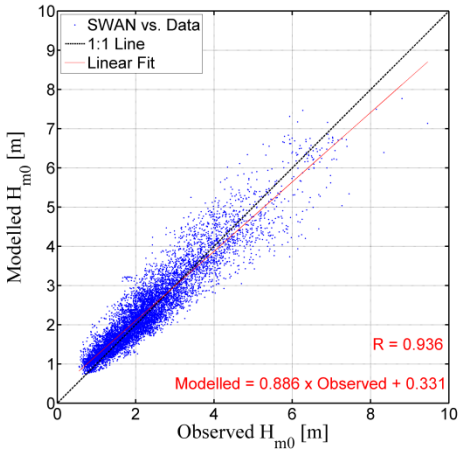

H_{m0}

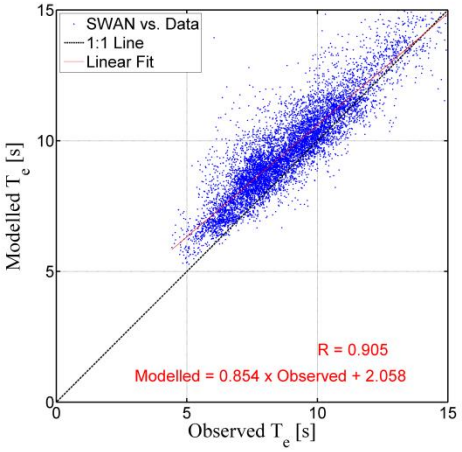

T_e

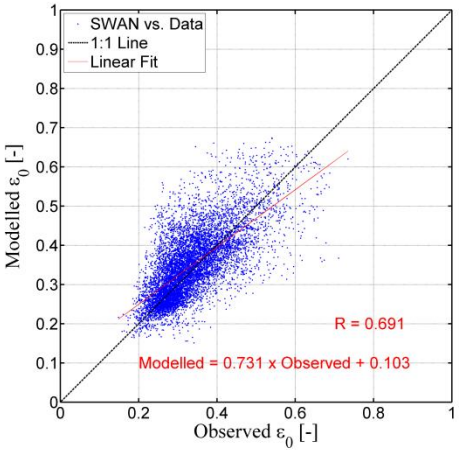

ε_0

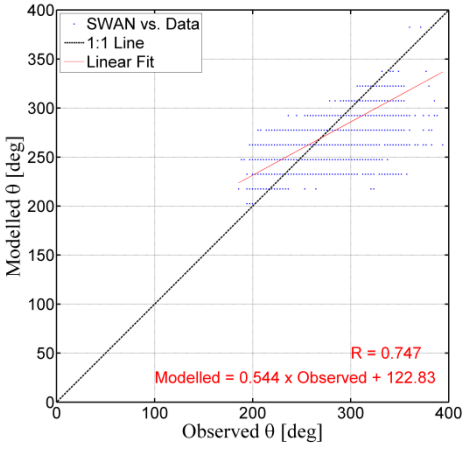

θ

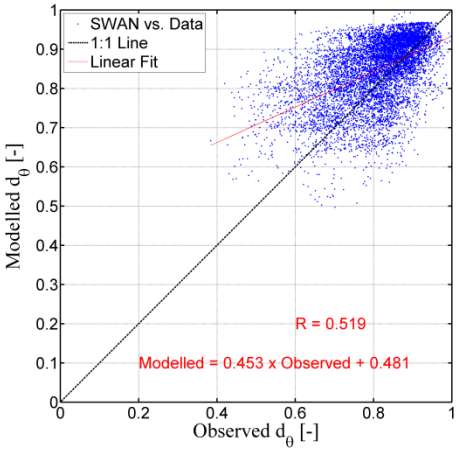

d_θ

Figure B.10. Scatter plots of IEC wave resource parameters for SWAN-NS, ST4 (29×24).

Appendix C

Performance Metrics Tables

Appendix C

Performance Metrics Tables

Table C.1. Performance metrics of the six IEC parameters for WWIII (ST2), SWAN-NS and SWAN-S results for baseline run (29×24).

Parameter	Model	RMSE	SI	Bias	Bias (%)	R
	WWIII	20	0.64	6.1	19.7	0.91
J (kW/m)	SWAN-NS	19	0.62	6.3	20.2	0.91
	SWAN-S	20	0.63	6.5	20.9	0.91
	WWIII	0.42	0.19	0.16	7.3	0.94
H_s (m)	SWAN-NS	0.44	0.20	0.18	8.1	0.94
	SWAN-S	0.45	0.20	0.19	8.4	0.94
	WWIII	0.98	0.11	0.50	5.6	0.90
T_e (s)	SWAN-NS	0.95	0.11	0.52	5.8	0.91
	SWAN-S	0.96	0.11	0.51	5.7	0.91
	WWIII	0.07	0.20	0.01	1.6	0.68
ϵ_0 (-)	SWAN-NS	0.06	0.19	0.00	0.7	0.72
	SWAN-S	0.07	0.20	0.00	1.1	0.71
	WWIII	22.87	0.08	-6.87	-2.4	0.74
θ (degrees)	SWAN-NS	22.24	0.08	-6.62	-2.3	0.75
	SWAN-S	22.62	0.08	-6.65	-2.3	0.74
	WWIII	0.10	0.13	0.05	6.2	0.48
d_θ (-)	SWAN-NS	0.10	0.12	0.04	5.1	0.55
	SWAN-S	0.10	0.12	0.04	5.0	0.55

Table C.2. Performance metrics of the six IEC parameters for WWIII, SWAN-NS and SWAN-S sensitivity runs (ST4-29×24).

Parameter	Model	RMSE	SI	Bias	Bias (%)	R
	WWIII	15.95	0.51	2.03	6.5	0.92
J (kW/m)	SWAN-NS	16.19	0.52	3.32	10.7	0.92
	SWAN-S	17.12	0.55	3.20	10.3	0.91
	WWIII	0.38	0.17	0.01	0.40	0.94
H_s (m)	SWAN-NS	0.41	0.18	0.07	3.3	0.94
	SWAN-S	0.43	0.19	0.07	2.9	0.93
	WWIII	1.23	0.14	0.86	9.7	0.90
T_e (s)	SWAN-NS	1.13	0.13	0.76	8.5	0.91
	SWAN-S	1.20	0.13	0.79	8.9	0.89
	WWIII	0.07	0.21	0.01	2.5	0.65
ϵ_0 (-)	SWAN-NS	0.07	0.20	0.01	4.0	0.69
	SWAN-S	0.07	0.21	0.01	4.3	0.67
	WWIII	23.44	0.08	-7.62	-2.7	0.73
θ (degrees)	SWAN-NS	22.62	0.08	-7.26	-2.5	0.75
	SWAN-S	23.08	0.08	-7.33	-2.6	0.73
	WWIII	0.10	0.13	0.05	5.8	0.44
d_θ (-)	SWAN-NS	0.10	0.12	0.04	4.8	0.52
	SWAN-S	0.10	0.12	0.04	4.8	0.51

Table C.3. Performance metrics of the six IEC parameters for WWIII sensitivity run (37×36).

Parameter	Model	RMSE	SI	Bias	Bias (%)	R
J (kW/m)	WWIII	20.95	0.67	6.75	21.65	0.91
	NA SWAN					
H_s (m)	WWIII	0.44	0.19	0.20	8.72	0.94
	NA SWAN					
T_e (s)	WWIII	0.90	0.10	0.36	4.07	0.91
	NA SWAN					
ϵ_0 (-)	WWIII	0.07	0.20	0.02	5.81	0.72
	NA SWAN					
θ (degrees)	WWIII	21.50	0.08	-5.81	-2.04	0.77
	NA SWAN					
d_θ (-)	WWIII	0.10	0.12	0.05	6.53	0.55
	NA SWAN					

Table C.4. Performance metrics of the six IEC parameters for WWIII sensitivity run (50×36).

Parameter	Model	RMSE	SI	Bias	Bias (%)	R
J (kW/m)	WWIII	21.10	0.68	6.80	21.80	0.91
	NA SWAN					
H_s (m)	WWIII	0.44	0.19	0.20	8.65	0.94
	NA SWAN					
T_e (s)	WWIII	0.90	0.10	0.38	4.31	0.91
	NA SWAN					
ϵ_0 (-)	WWIII	0.07	0.20	0.02	5.82	0.72
	NA SWAN					
θ (degrees)	WWIII	21.43	0.08	-5.79	-2.03	0.77
	NA SWAN					
d_θ (-)	WWIII	0.10	0.12	0.05	6.56	0.55
	NA SWAN					

Distribution

No. of
Copies

Name
Organization
Address
City, State and ZIP Code

Organization
Address
City, State and ZIP Code
Name
Name
Name
Name
Name (#)

Name
Organization
Address
City, State and ZIP Code

No. of
Copies

 # Foreign Distribution

Name
Organization
Address
Address line 2
COUNTRY

 # Local Distribution

Pacific Northwest National Laboratory

Name	Mailstop
Name	Mailstop
Name	Mailstop
Name	Mailstop
Name	(PDF)